Signal propagation and entrainment of Denmark Strait Overflow Water as measured at Ammassalik, 2007-2012

vorgelegt von

Manuela Köllner

Masterarbeit im Fach Physikalische Ozeanographie

verfasst an der Fakultät für Mathematik, Informatik und Naturwissenschaften

im Fachbereich Geowissenschaften,

Centrum für Erdsystemforschung und Nachhaltigkeit,

Institut für Meereskunde

der Universität Hamburg

Hamburg

Oktober 2012

Thema: On the variations of the Denmark Strait Overflow Water at Angmagssalik

Supervisors:

Prof. Dr. Detlef Quadfasel
Dr. Kerstin Jochumsen

Abstract

Changes in the water mass characteristics of the Denmark Strait Overflow Water (DSOW) can influence the North Atlantic Deep Water which is an important component of the Atlantic Meridional Overturning Circulation. Temperature and salinity data from mooring arrays at the Denmark Strait sill and near Ammassalik between 2007 and 2012 were analyzed to quantify changes in hydrographic properties and to identify their sources. No trends in the potential temperature and salinity time series were detected. High variability on short time scales is present at the moorings, but in the power spectra no dominant frequency is evident. A seasonal cycle can be detected in all time series, but can only explain up to 10% of the variance. Two freshening events can be identified in April to June 2011 and in January 2012. Both reach about half the magnitude as the ones detected in 1999 and 2004. For potential temperature no outstanding events were recognized. The DSOW potential temperature time series of the Denmark Strait and Ammassalik array show good correlation. Temperature signals are thus advected from the Denmark Strait to the Ammassalik array. Salinity signals at Ammassalik can not be traced to the sill. Hence salinity signals are not advected from the Denmark Strait. Entrainment of warm and salty Atlantic water and fresh East Greenland Current (EGC) water can explain the whole range of temperature and salinity changes in the DSOW. Changes in the EGC can hence strongly influence the salinity variability, as was suggested in earlier studies. Salinity minima can therefore result from higher entrainment rates of EGC water.

Zusammenfassung

Änderungen in der Wassermassencharakteristik des Dänemarkstraßen Overflow Wassers (DSOW) können das Nord Atlantische Tiefenwasser beeinflussen, welches ein wichtiger Teil der Atlantischen Meridionalen Overturning Zirkulation ist. Temperatur- und Salzgehaltsdaten von Verankerungen an der Schwelle der Dänemarkstraße und nahe Ammassalik zwischen 2007 und 2012 werden analysiert um Änderungen in den hydrographischen Eigenschaften des DSOW zu quantifizieren und ihren Ursprung zu identifizieren. In den Zeitserien für potentielle Temperatur und Salzgehalt sind keine Trends ersichtlich. Hohe Variabilität auf kurzen Zeitskalen ist an den Verankerungen vorhanden, aber in den Energiespektren ist keine dominante Frequenz erfaßbar. In allen Zeitserien kann ein Jahresgang festgestellt werden, der allerdings nur bis zu 10% der Varianz in den Zeitserien erklären kann. Zwei signifikante Ereignisse mit geringen Salzgehalten können von April bis Juni 2011 und im Januar 2012 identifiziert werden. Beide erreichen etwa die Hälfte des Ausmaßes der beiden Ereignisse 1999 und 2004. In der potentiellen Temperatur wurden keine bedeutenden Ereignisse entdeckt. Die DSOW Temperaturzeitserien zwischen der Dänemarkstraßenschwelle und den Verankerungen nahe Ammassalik korrelieren gut, woraus folgt, dass Temperatursignale von der Schwelle nach Süden transportiert werden. Signale im Salzgehalt nahe Ammassalik können nicht zur Schwelle zurückverfolgt werden. Die Signale im Salzgehalt werden also nicht von der Schwelle advehiert. Die Einmischung von warmem salzreichen Atlantischen Wasser und salzarmen Wasser aus dem Ostgrönlandstrom kann den ganzen Umfang an Temperatur- und Salzgehaltsänderungen des DSOW erklären. Wie in früheren Studien bereits angenommen, können Änderungen im Wasser des Ostgrönlandstroms somit die Variabilität des Salzgehaltes beeinflussen. Minima im Salzgehalt können also aus einer größeren Einmischungsrate von Wasser aus dem Ostgrönlandstrom resultieren.

Contents

List of Figures

List of Tables

List of Abbreviations

ADCP	Acoustic Doppler Current Profiler
AMOC	Atlantic Meridional Overturning Circulation
ASOF	Arctic-Subarctic Ocean Fluxes
CEFAS	The Centre for Environment, Fisheries & Aquaculture Science
CFC	Chlorofluorocarbon
CIS	Central Irminger Sea
CTD	Conductivity-Temperature-Depth sensor
DS	Denmark Strait
DSOW	Denmark Strait Overflow Water
EGC	East Greenland Current
FBC	Faroe Bank Channel
GEOMAR	Helmholtz-Zentrum für Ozeanforschung Kiel
ISOW	Iceland-Scotland Overflow Water
LOCO	Long-term Ocean Climate Observation
LS	Labrador Sea
LSW	Labrador Sea Water
NADW	North Atlantic Deep Water
NEADW	North East Atlantic Deep Water
THOR	Thermohaline Overturning - at Risk?
VEINS	Variability of Exchanges in the Northern Seas

1 Introduction

The moderate climate in Europe is highly influenced by the northward heat transport in the atmosphere and ocean from the tropics and the South Atlantic Ocean. The **A**tlantic **M**eridional **O**verturning **C**irculation (**AMOC**) provides one-quarter of the global meridional heat transport (Kanzow et al., 2007). Warm surface water is transported from the south to higher latitudes where it is loosing heat to the atmosphere. Thereby the density increases and the water sinks to feed a deep returning flow which transports the **N**orth **A**tlantic **D**eep **W**ater (**NADW**).

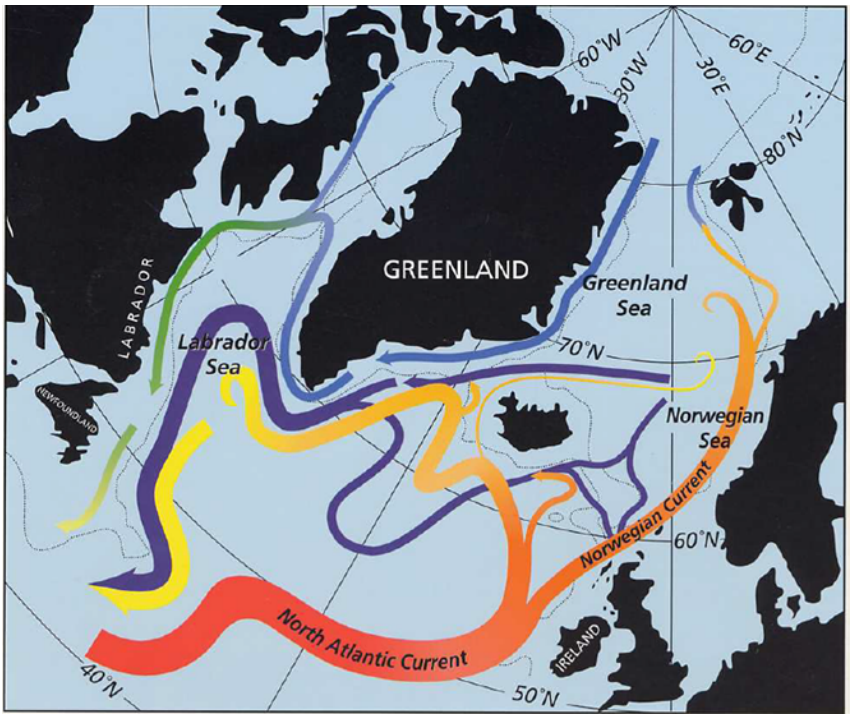

Figure 1: *Sketch of the North Atlantic Current System from (McCartney et al., 1997). The North Atlantic Current (red) transports warm water near the surface to higher latitudes. One of its branches is flowing west-southward steered by topography until it reaches the Labrador Sea (light orange - yellow). This part forms the subpolar gyre. The other branch feeds the Norwegian Atlantic Current (orange). The compensating dense flows (blue) are flowing southward at depth, crossing the ridge system between Greenland, Iceland and Scotland and descend into the deep ocean where they contribute to the North Atlantic Deep Water.*

Figure 1 shows a sketch of the North Atlantic Current System. Most of the conversion from surface waters to deeper layers occurs in the Labrador Sea and the Nordic Seas (Iceland Sea, Greenland Sea and Norwegian Sea) (Talley et al., 2011). The North Atlantic Current (Figure 1, red arrow) transports warm water from the subtropical gyre to higher latitudes. When it reaches the Greenland-Scotland-Ridge, which separates the North Atlantic from the Nordic Seas, the North Atlantic Current feeds into the Norwegian Atlantic Current. The Norwegian Atlantic Current (Figure 1, orange arrow) flows further north along the coast of Norway. The other branch of the North Atlantic Current follows the topography along the Greenland-Scotland-Ridge and Reykjanes Ridge south of Iceland (Figure 3) until it reaches the Labrador Sea (Figure 1, orange and yellow arrow) (Talley et al., 2011). In the Labrador Sea deep convection occurs (Figure 1, yellow arrow).

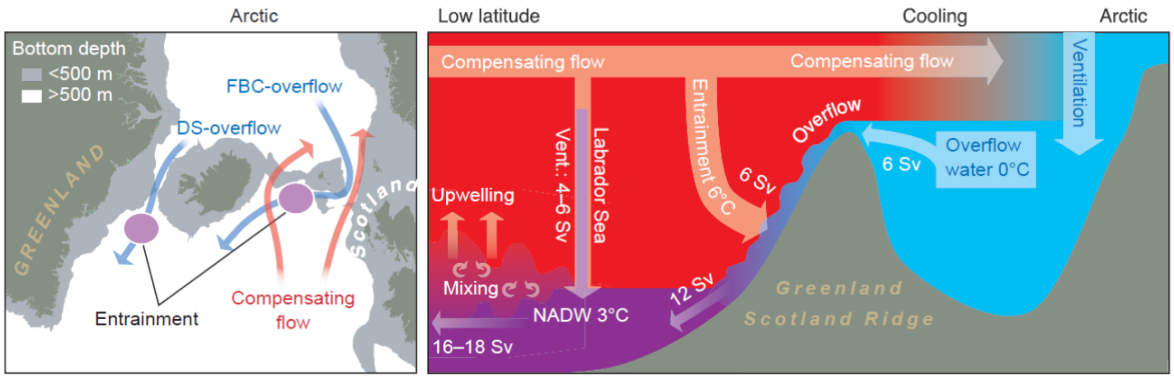

Figure 2: *Exchange of water across the Greenland-Scotland Ridge from Hansen et al. (2004). Left: Main flows over the Greenland-Scotland Ridge. The overflows through Denmark Strait (DS) and the Faroe Bank Channel (FBC) are shown in blue and the compensating flow at the surface is marked in red. Right: The schematic shows the formation of North Atlantic Deep Water (NADW). Dense water is produced at polar latitudes. It spreads equatorward through the deep passages in the Greenland-Scotland-Ridge and descends into the deep North Atlantic. While descending ambient water is entrained, which leads to a modification of the water characteristics and an increase in volume transport. Together with the ventilated Labrador Sea Water (LSW) the overflows are feeding the NADW.*

The deep large scale meridional pressure gradient drives a southward flow as a result of the density difference between the dense source water in the north and the less dense water in the downstream reservoir. Dense waters are flowing from the Nordic Seas over the Greenland-Scotland-Ridge through a few deep passages into the North Atlantic (Figure 1,

blue arrow). Figure 2 (right) shows the exchange of water over the Greenland-Scotland-Ridge more in detail. The overflow is steered by topography (Talley et al., 2011). It descends as a plume due to its high density and is mixed with ambient water on the way into the deep ocean (Voet, 2006). The entrainment of ambient water leads to a modification of temperature, salinity and other characteristics of the overflow plume and the volume transport is almost doubled. In the deep ocean the modified overflow water is feeding the NADW (Hansen et al., 2004).

Changes in the deep southward flows of the AMOC can have a resulting change in the strength of the northward flows. A change in the strength of the northward flows could then lead to a change of heat transport to higher latitudes and thus to a change of the European climate. Therefore the North Atlantic is a favored research area.

The northern overflows are the densest water masses in the subpolar North Atlantic. The variability and the entrainment processes, while they are descending into the deep ocean, are not fully understood yet. In this thesis the variability of the Denmark Strait Overflow Water between the Denmark Strait sill and the Ammassalik array, approximately 500 km south of the Denmark Strait, between 2007 and 2012 will be analyzed. By correlating the data from Denmark Strait and Ammassalik it is possible to observe signals in temperature and salinity to obtain a better understanding of the advection and entrainment of the DSOW. Changes in hydrographic properties will be quantified and their sources will be identified.

1.1 The northern Overflows

The Greenland-Scotland-Ridge is an underwater mountain system, which reaches from Greenland via Iceland and the Faroe Islands to Scotland and separates the North Atlantic from the Nordic Seas (Figure 3). It blocks the outflow of dense water from the Nordic Seas. The mean water depth over the ridge is approximately 500 m. Only a few passages are deeper and allow an outflow of dense water. The most important passages are the Denmark Strait, which is located between Greenland and Iceland, with a sill depth of approximately 650 m and the Faroe Bank Channel, between the Faroe Islands and Scotland, with a sill depth of approximately 840 m (Voet, 2006). The water masses

reaching the North Atlantic over these sills are called **D**enmark **S**trait **O**verflow **W**ater (**DSOW**) and **I**celand-**S**cotland **O**verflow **W**ater (**ISOW**) (Fig. 2 left). After passing the sill the DSOW descends into the Irminger Basin (Voet, 2006). The Irminger Basin is bounded by Greenland in the west and by the Reykjanes Ridge in the east. The ISOW is descending into the Iceland Basin, which is bounded by the Reykjanes Ridge in the west and the Rockall Plateau in the east.

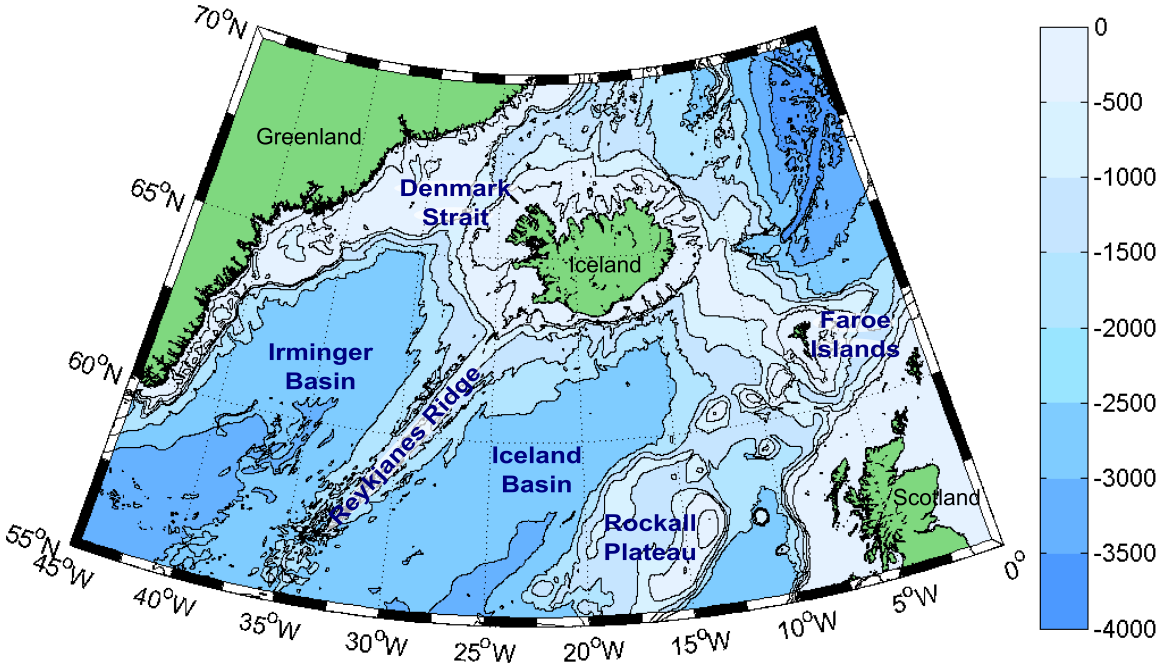

Figure 3: *Topography of the Irminger Basin, Iceland Basin and passages between the Nordic Seas and the North Atlantic.*

The Denmark Strait Overflow Water is defined as a water mass with a potential density anomaly of more than 27.8 kg/m^3 and a potential temperature less than 2°C at the Denmark Strait sill (Tanhua et al., 2005). Thus, it is the densest water mass found in the Irminger Basin. For the region near Ammassalik (old spelling: Angmagssalik)[1] the near-bottom layer of the DSOW is defined as water with potential density anomalies

[1]Ammassalik, also called Tasiilaq, is a town at the southeastern coast of Greenland, located at the Ammassalik fjord. The spelling of the town changed during the last years from Angmagssalik to Angmassalik and the now used Ammassalik. In this thesis the new spelling Ammassalik is used.

$> 27.85\ kg/m^3$. The different density intervals of the overflow layers were defined mainly from the distribution of the tracer sulphur hexafluoride (SF6) and partly from hydrographic analysis (Dickson et al., 2008). The plume passes the Greenland-Scotland-Ridge in pulses. The bottom part of the plume is almost homogeneous and cold. The upper part is a temperature-stratified layer which is covered by a low salinity lid (Dickson et al., 2008). The dense water transport at the sill is around 3.4 Sv (Jochumsen et al., 2012) which increases further downstream up to 10.7 Sv near Ammassalik due to entrainment (Dickson et al., 2008). The transport, velocity and water mass characteristics are influenced by entrainment. The width of the Denmark Strait is larger than the barocline Rossby radius, which is 14 km at these latitudes (Whitehead, 1998). This allows the formation of meso-scale eddies. They have a period of 2-10 days at the Denmark Strait sill (Moritz, 2011). They can also be formed during the descending of the DSOW south of the sill. These eddies have a period of 2-5 days (Voet and Quadfasel, 2010). The DSOW is topographically steered and follows the west Greenland continental slope. The velocity of the DSOW is typically 50 cm/s but can be up to 100 cm/s (Macrander et al., 2007). Near the sill, the DSOW layer thickness varies between 50 to 300 m (Macrander et al., 2007). The DSOW layer thickness decreases south of the sill (Käse et al., 2003). At the Ammassalik array, approximately 500 km downstream of the sill, the DSOW reaches a depth of about 2000 m (Voet and Quadfasel, 2010).

1.2 Entrainment processes

The entrainment of ambient water into the plume can be separated into two main processes: vertical and horizontal mixing, which are shown in Fig. 4. In the left of Figure 4 turbulent (vertical) mixing is shown. It is induced by vertical velocity shear between the overflow plume and ambient water which leads to vertical instabilities and to breaking internal waves (Kelvin-Helmholtz instabilities). This mechanism is explained in detail in Figure 5. Figure 5a shows two different water layers. The upper one is of lower density and is moving with higher velocities than the underlying layer with higher density. The two layers are moving in opposite directions. The process also works with movement into the same direction but with different velocities of the layer. The steps b to d show that the shear between the layers produces a local instability which grow to billows (Figure 5e). The billows are breaking up which leads to turbulent mixing of water above and below the interface (Figure 5f).

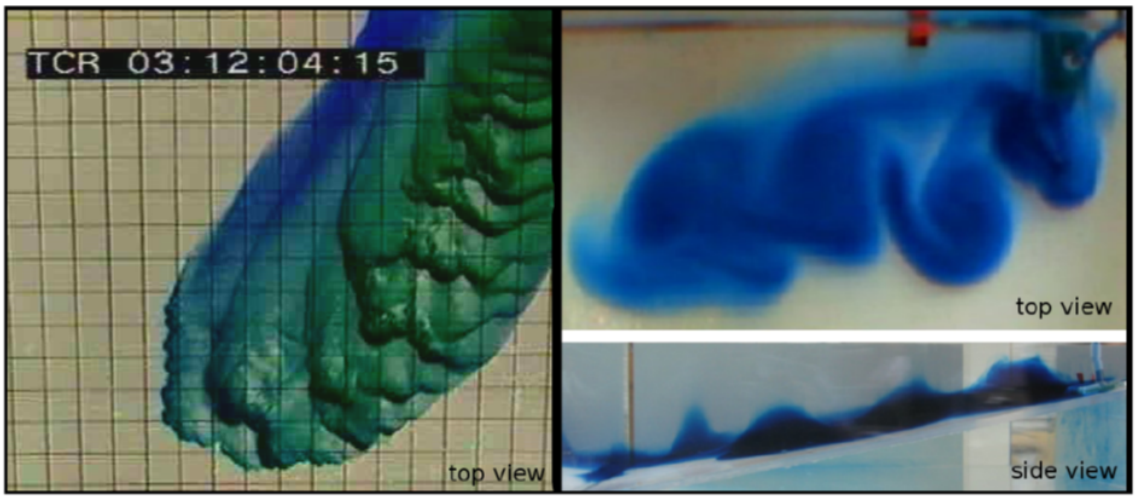

Figure 4: *Entrainment processes shown in a rotating tank experiment from Voet (2006). Left: Water with a high density (green colored) contrast to the surrounding water descends at a sloping plane. The plane is high at the upper image border and low at the lower image border. Vertical turbulent mixing due to breaking internal waves is visible through the variations in the plume color. Right: Horizontal mixing by meso-scale eddies due to a low density contrast. The upper image shows the top view where vortices can be recognized, which stir ambient water into the dense plume. The lower image shows the side view to give an impression of the vertical structure of the plume.*

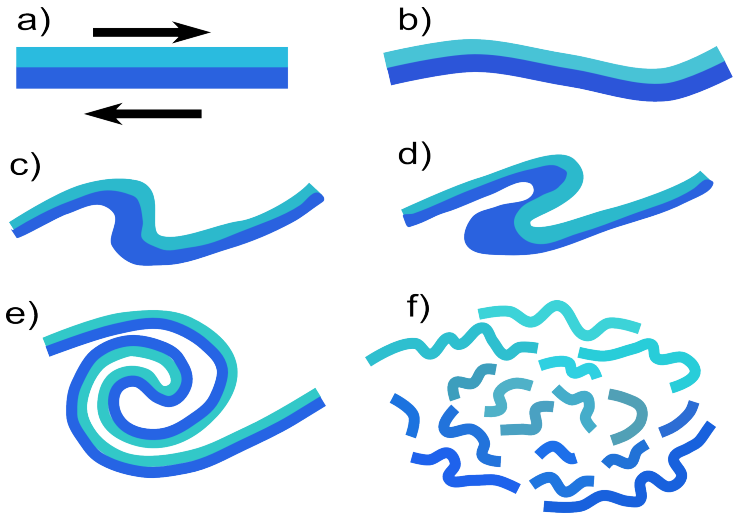

Figure 5: *Mixing by breaking internal waves. a) shows a layer of low density water with high velocities over a layer of high density water with less velocity. The layers are moving in opposite directions. The steps b-f show the loosing of coherence of the two layers and the break up into turbulent patches.*

On the right-hand side of Figure 4 horizontal mixing is shown. While the DSOW is descending, meso-scale vortices are formed. These meso-scale eddies can induce lateral stirring, which horizontally transports ambient water into the plume. In vortices like eddies, kinetic energy is dissipated and transformed into another form of energy like thermal energy. Voet and Quadfasel (2010) found out that the DSOW is warmed by entrainment through meso-scale eddies, with highest warming rates within the first 200 km downstream of the sill.

1.3 Water masses contributing to the DSOW

Tanhua et al. (2005) described the composition of the Denmark Strait Overflow Water between the Denmark Strait and 360 km downstream of the sill. The results were used to calculate the entrainment of ambient water into the overflow plume in the northern Irminger Basin. For the analysis they used the optimum multi parameter analysis with the following parameters

- Potential temperature,
- Salinity,
- Oxygen,
- Nitrate,
- Phosphate,
- Silicate,
- CFCs.

They found out that the DSOW at the Denmark Strait sill consists of seven different water masses. The ratios of the contributing water masses are changing over the different years of measurements. This could be a result of different sampling locations, but also a result of actual changes in the individual source water mass compositions. Nevertheless, the range of ratios of the contributing water masses was similar over the whole time period of observations. DSOW at the sill consists of 5-12 % upper Polar Deep Water, 22-34 % Recirculated Atlantic Water, and 4-12 % Polar Surface Water, all transported

by the East Greenland Current. Other contributing water masses are 9-17 % Greenland Sea Arctic Intermediate Water formed in the Greenland Sea and 5-6 % Iceland Sea Arctic Intermediate Water built in the Iceland Sea, together named Arctic Intermediate Water. Furthermore, it consists of 18-31 % Arctic Deep Water formed in the Arctic Ocean and 7-15 % Arctic Atlantic Water, which is modified Atlantic Water after entering the Arctic Ocean.

Further south, 360 km downstream of the Denmark Strait sill, the water masses contributing to the DSOW differ due to entrainment along the way south. It now consists of 18 % dense Arctic Ocean Water, 20 % Arctic Intermediate Water from the Nordic Seas, 32 % modified Atlantic Water, and 30 % water entrained south of the sill from different water masses. The Middle Irminger Water was detected to be the most important water mass to entrain into the overflow plume close to the sill. After the plume reached larger depth further south of the sill, Labrador Sea Water and modified ISOW become the most important entrained water masses (Tanhua et al., 2008). Due to circulating around the Reykjanes Ridge the ISOW is also called North East Alantic Deep Water (NEADW).

De Jong (2010) found out that convective mixing down to 500 m depth occurred in the Irminger Sea during winter times between 2004 and 2008. The deepest mixed layer found in the Irminger Sea in the winter 2007-2008 reached a depth of 1000 m. This deep convection can effect the entrainment into the DSOW near the Denmark Strait sill as well, because it changes the Middle Irminger Water. The exact contribution of every water mass to the entrainment is yet unknown. To figure out which water masses are mostly contributing to the entrainment into the DSOW, temperature and salinity properties of the DSOW have to be analyzed.

1.4 Studies on the variability of the Denmark Strait Overflow plume

Past studies on the Denmark Strait Overflow plume show high variability in velocity and temperature measurements, as well as in salinity measurements. Ross (1984) detected high variability on timescales of 2-5 days near the Denmark Strait sill. Dickson and Brown (1994) pointed out that there is high variability on timescales of 1-12 days about 500 km downstream of the sill, near Ammassalik.

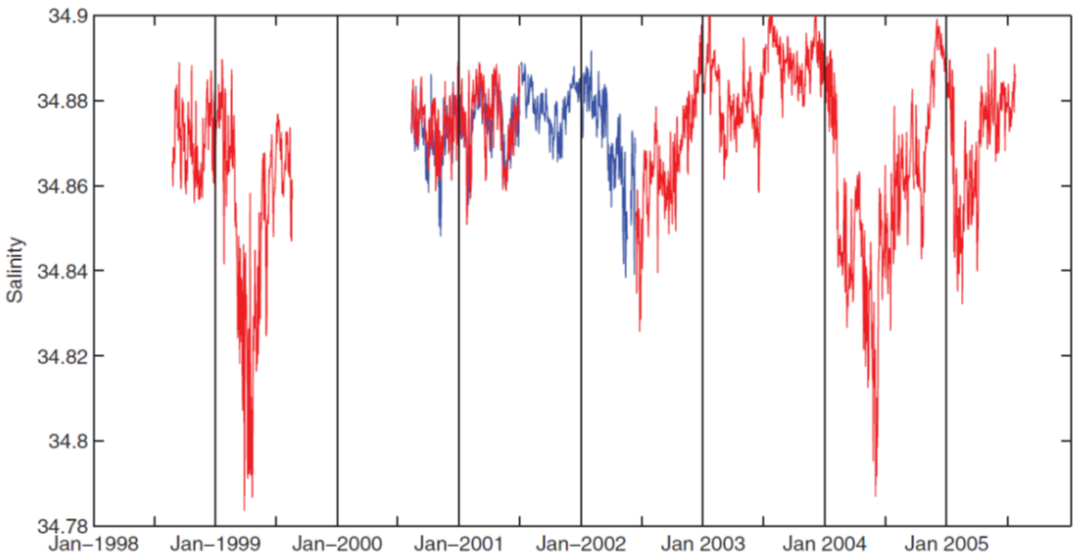

Figure 6: *Salinity time series of the DSOW at Ammassalik between 1998 and 2006 from Dickson et al. (2008). Extreme freshening events with a freshening of up* 0.1 *psu show up in spring 1999 and late spring 2004.*

Dickson et al. (2008) recognized a series of freshening events in the overflow plume between 1998 and 2006 (Figure 6). In spring 1999 and late spring 2004 extreme freshening events occurred with a freshening of around 0.04 *psu* to 0.06 *psu* over a period of one month or longer (Hall et al., 2011) peaking up to 0.1 *psu* (Dickson et al., 2008). The salinity minima coincided with long-term minima in the overflow temperature. They assumed the source for these freshening events to be further upstream. One hypothesis was the strengthening of freshwater input fed by the East Greenland Current (Holfort and Albrecht, 2007). Rudels et al. (2002) pointed out that the variability of the DSOW plume is caused by an increase in volume flux of low salinity water from north of the Denmark Strait sill. This low salinity water is transported by the East Greenland Current towards the Denmark Strait sill. Model analysis by Hall et al. (2011) showed that the reason for the increase of low salinity water is an increase in southward wind stress parallel to the east Greenland coast. According to this analysis the detected freshening events and variability in salinity and temperature off Ammassalik are resulting from advection from the Denmark Strait sill.

But is advection the main reason for the variability at the Ammassalik array? The entrainment into the plume on its way south almost doubles the volume transport of the plume (Voet and Quadfasel, 2010), which could also induce variability of the temperature and salinity properties. Until now the exact volume increase by entrainment is unknown, as well as the changes of DSOW properties due to entrainment.

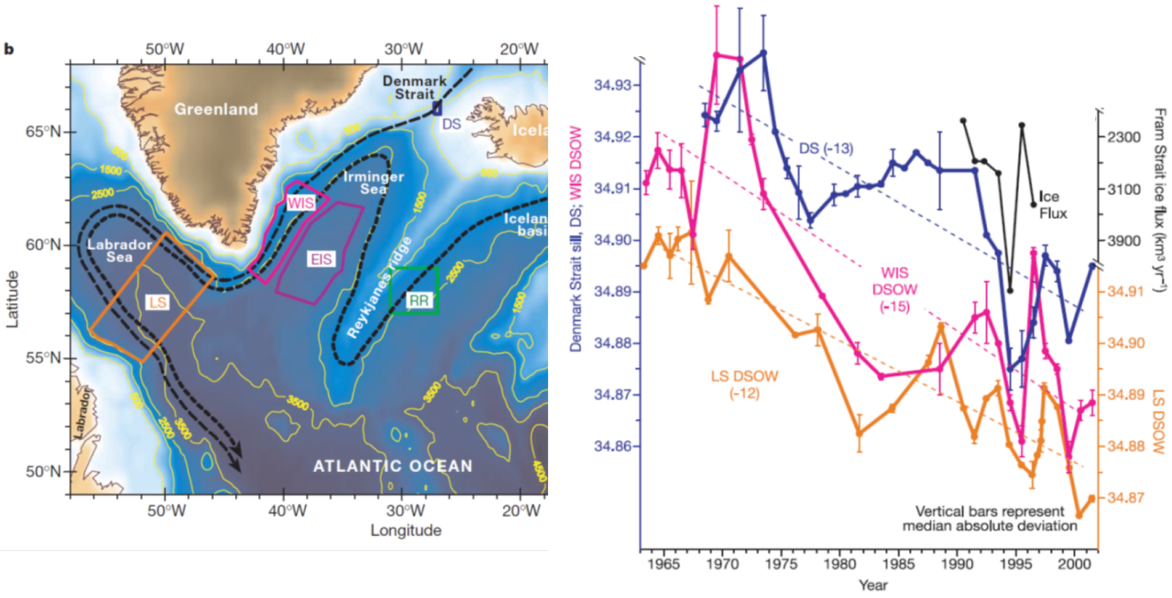

Figure 7: *DSOW salinity time series from Dickson et al. (2002). The time series are plotted to a common scale and are color- and letter-coded to identify their location marked in the map on the left. The curve DS (Denmark Strait) describes the salinity trends of the DSOW at the sill at a depth between 500-550 m with temperatures* $< 0°C$*. The WIS DSOW (DSOW in the western Irminger Sea) and LS DSOW (DSOW in the Labrador Sea) describe the salinity trends of the DSOW in the near bottom layer further south, where the plume descends the slope off southeast Greenland. The black curve shows the observed annual mean ice flux through the Fram Strait between 1990 and 1997 for comparison.*

Furthermore Dickson et al. (2002) detected a freshening trend of the deep water masses in the North Atlantic, especially of the DSOW at the Denmark Strait sill and further downstream (Figure 7). This freshening trend and anomalies of the DSOW have been attributed to increasing freshwater input from higher net precipitation, sea ice melt or glacial run-off into the Nordic Seas. With the present time series of the Ammassalik array and Denmark Strait sill moorings we can now monitor if the detected trend continued between 2007 and 2012.

The aim of this thesis is to answer some of the still remaining questions about the Denmark Strait Overflow plume.

- Can the freshening trend detected by Dickson et al. (2002) also be seen in the data between 2007 and 2012?
- What kind of variability in salinity and temperature occurs between 2007 and 2012 at the Ammassalik array?
- Did extreme events in salinity and temperature occur between 2007 and 2012 at the Ammassalik array, as seen in 1999 and 2004 by Dickson et al. (2008)?
- Are salinity and temperature signals advected from the Denmark Strait to the Ammassalik array?
- Which water masses have to be entrained into the DSOW to change the salinity and temperature variability of the plume?

Chapter two gives a brief overview about the instruments used for measuring as well as the data processing, quality control and the analysis methods. The third chapter describes the time series of salinity and potential temperature measured in the Denmark Strait and at the Ammassalik array between 2007 and 2012. Detected trends and variabilities of the time series are discussed. Freshening events are identified and described. Chapter four shows the correlations between the time series of the Denmark Strait and Ammassalik array to infer the influence of the entrainment between the two locations. Entrained water masses are identified and their volume contents are approximated in chapter five. A conclusion is given in chapter six.

2 Instruments, data processing and methods

In this thesis measurements from moored instruments between 2007 and 2012 are used. The measuring periods are 1-2 years and the temporal resolution is 10-20 minutes. To detect all scales of variability, a good temporal resolution as well as a long measuring period is needed. This shows and explains the positions and instruments of the moorings in the Ammassalik and Denmark Strait arrays. It shows the result of the quality control of the data and explains the different steps and methods used to analyze the temperature and salinity time series with MATLAB. The methods used for correlation and analyzing the contributions of different water masses to the entrainment into the DSOW are explained.

2.1 Mooring design

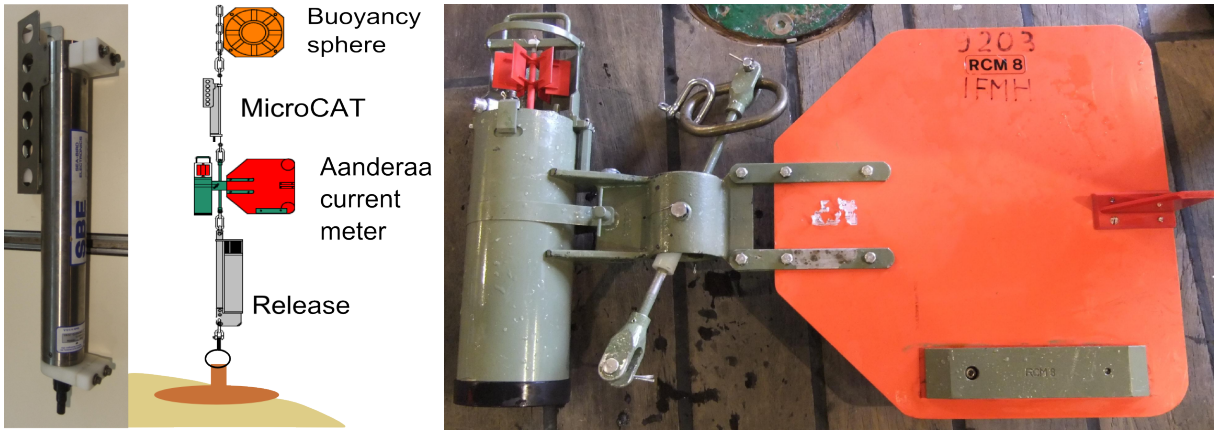

Figure 8: *Example of the mooring design. The moorings in the Ammassalik array are equipped with 2-3 Aanderaa current meters (right) and SeaBird SBE37SM MicroCATs (left) at different depth levels near the bottom. The MicroCATs are always located above the current meters.*

The data used in this thesis are from moorings which were equipped with Aanderaa current meters, as well as SeaBird SBE37SM MicroCATs (Figure 8). Aanderaa RCM-8 current meters are mechanical current meters with a recording unit and a vane. While the vane rotates the current meter into the direction of the current, the propeller of the recording unit measures the speed of the current. A compass is inside the recording unit to determine the direction of the current from the orientation of the vane relative to the

compass. The recording unit is also equipped with a temperature sensor. The accuracy of the instruments is for velocities $\pm 1 \frac{cm}{s}$, $\pm 5°$ for the direction and $\pm 0.05°C$ for temperature measurements. In some moorings Aanderaa RCM-11 acoustic current meters were used. They produce a sound signal which is backscattered by particles or air bubbles in the water column. The frequency shift of the incoming reflection is measured for four directions. The direction of the current is detected by measuring along two orthogonal axes. A tilt sensor compensates the tilt. The vector averaged current speed and direction over the last sampling interval is computed by a microprocessor (Aandera, 2002).

MicroCATs are measuring temperature and conductivity. The salinity of the sea water can be calculated from the conductivity measurements. The accuracy of the factory calibrated MicroCAT measurements is $0.002°C$ for temperature and 0.0015 psu for salinity. MicroCATs can be equipped with an additional pressure sensor which gives the exact depth of the MicroCAT in the water column. The instruments are attached to a kevlar rope with buoyancy spheres at the top of the mooring and above every group of instruments. The spheres keep the mooring in a vertical position. The mooring is fixed at the seafloor with a heavy weight. An acoustic release between the mooring and the anchor allows to recover the instruments after the measurement period (Figure 8). An acoustic signal is sent to the release from the ship which leads the releaser to disconnect the rope from the anchor.

The Ammassalik array was set up in 1986 by the Lowestoft Laboratory off Ammassalik in the east of Greenland at 63°N. It has been maintained to present by an UK, German and Finnish team within the EU-funded projects VEINS (1997-2000), ASOF (2003-2005) and THOR (2008-2012). The moorings are typically recovered and deployed in a one year interval. The array consisted of up to eight current meter moorings partly also equipped with MicroCATs. Data of four moorings between 2007 and 2012 are analyzed within this thesis. The moorings were deployed at the continental slope approximately 500 km south of the Denmark Strait sill to cover the dense overflow water from the Denmark Strait as seen in Figure 9 (Dickson et al., 2008).

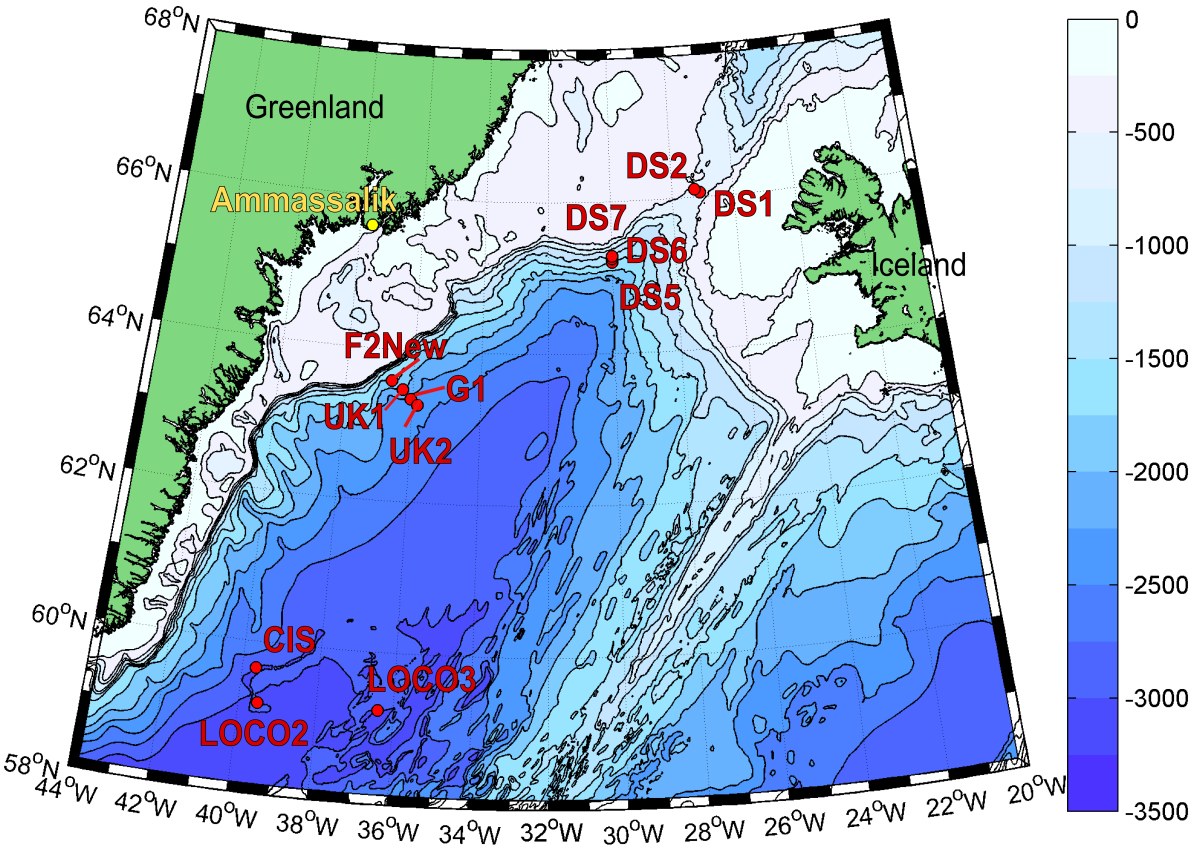

Figure 9: *Locations of the moorings.*

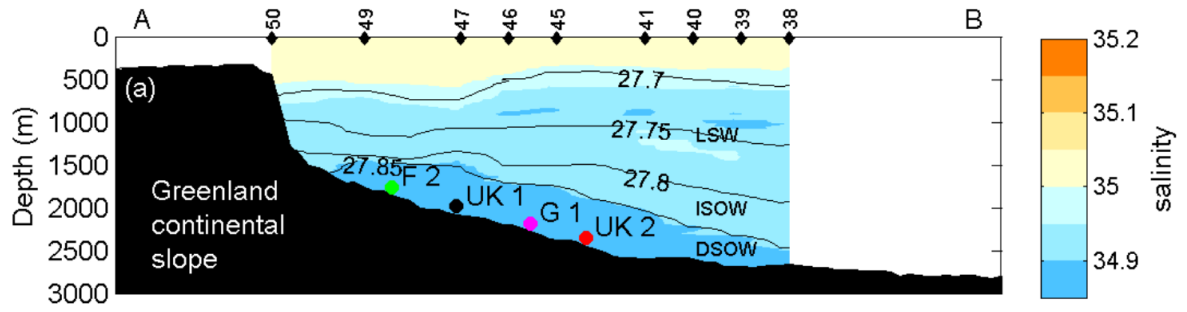

Figure 10: *Salinity section obtained from CTD casts during June 2009 by the MSM12-1 cruise at the Ammassalik array from Hall et al. (2011). The location of the moorings F2, UK1, G1 and UK2 are marked with dots. Isopycnals allow to discern the water masses present at the array.*

Figure 10 shows a vertical section through the Ammassalik array obtained from CTD casts during the RV Maria S. Merian 12-1 cruise in June 2009 by (Hall et al., 2011). The water mass at the bottom can be identified as DSOW. Between the 27.8 and the 27.85 isopycnal Iceland-Scotland Overflow Water is located. It is characterized by densities $> 27.8\ kg/m^3$ and a salinity between 34.91 *psu* and 34.93 *psu* after it circulated around the Reykjanes Ridge (Fogelqvist et al., 2003).

Above the ISOW layer **L**abrador **S**ea **W**ater (LSW) is found. LSW and ISOW are separated by the 27.8 isopycnal. The upper limit of LSW is at a depth of about 500 m at the 27.7 isopycnal (Hall et al., 2011). The moorings are located in the core of the dense overflow. The salinity and temperature data from MicroCATs are usually calibrated against CTD data obtained at each mooring deployment and recovery.

Table 1: *Locations of the moorings equipped with MicroCATs*

Array	**Mooring**	**Latitude**	**Longitude**	**Depth**	**time period**
Ammassalik	F2New	63° 35.5' N	36° 39' W	1780 m	2009-2012
Ammassalik	UK1	63° 29' N	36° 18' W	1980 m	2007-2012
Ammassalik	G1	63° 22' N	36° 04' W	2200 m	2009-2012
Ammassalik	UK2	63° 17' N	35° 52' W	2350 m	2007-2012
Denmark Strait	DS1	66° 04.72' N	27° 04.89' W	660 m	2007-2012
Denmark Strait	DS2	66° 07.25' N	27° 16.21' W	570 m	2007-2012
Denmark Strait	DS5	65° 11.97' N	30° 00.1' W	1500 m	2010-2011
Denmark Strait	DS6	65° 14.51' N	30° 00.0' W	1400 m	2010-2011
Denmark Strait	DS7	65° 16.93' N	30° 00.1' W	1300 m	2010-2011
LOCO	LOCO2	59° 12.2' N	39° 30.3' W	3000 m	2007-2011
LOCO	LOCO3	59° 13.0' N	36° 19.9' W	3000 m	2007-2011
CIS	CIS	59° 41.0' N	39° 43.0' W	2800 m	2007-2010

At Denmark Strait, the mooring array consists of short moorings with an Acoustic Doppler Current Profiler (ADCP) on the top and MicroCATs beneath, as well as a release. They are located at the Denmark Strait sill at approximately 660 m and 570 m depth (Figure 9).

Table 1 gives an overview of the location of the moorings equipped with MicroCATs in the deployment period between 2007 and 2012 used for this thesis and shown in Figure 9.

For this study data from the moorings F2New, UK1, G1, UK2, DS1, and DS2 in the time period between 2007 and 2012 are used. The G1 and DS2 moorings are provided by the Institut für Meereskunde, Hamburg, Germany. The UK1 and UK2 moorings are provided by The **C**entre for **E**nvironment, **F**isheries & **A**quaculture **S**cience (**CEFAS**). The F2New mooring is provided by the Finnish Institute of Marine Research and the DS1 mooring is provided by the Marine Research Institute, Iceland.

For the water mass analysis, data from the moorings LOCO2, LOCO3, CIS, DS5, DS6 and DS7 are used in addition. The LOCO (Long-term Ocean Climate Observation) moorings are provided by the Royal Netherlands Institute for Sea Research. The MicroCAT of the LOCO2 mooring is located in the DSOW core near Cape Farewell at the 3000 m isobath. The LOCO3 mooring is located further east, close to the Reykjanes Ridge near the 3000 m isobath. The CIS (Central Irminger Sea) mooring is provided by the Helmholtz-Zentrum für Ozeanforschung Kiel (GEOMAR). It is located in the central Irminger Sea north of LOCO2. One of its MicroCATs is measuring at 1000 m depth, where the LSW can be located. The Denmark Strait moorings DS5, DS6 and DS7 are provided by the Institut für Meereskunde, Hamburg. They are located 100 km south of the Denmark Strait sill in a depth of 1300 - 1500 m.

2.2 Data processing

The data from the moorings DS5, DS6 and DS7 were calibrated and quality controlled by the Institut für Meereskunde Hamburg. The data from the LOCO moorings were calibrated, quality controlled and calculated to one day means by the Royal Netherlands Institute for Sea Research and the CIS data by the GEOMAR.

The MicroCAT data shown in Table 2 are available as Ascii files. 24 time series are calibrated with CTD data, seven time series are from MicroCATs which were factory calibrated by SeaBird. The MicroCAT data are calibrated to reduce errors due to sensor drift.

Table 2: *MicroCAT data from the Denmark Strait sill and Ammassalik moorings between 2007-2012. The P behind a depth indicates that the MicroCAT were equipped with a pressure sensor.*

Mooring	**Year**	**Number of MicroCATs**	**Depth of MicroCATs [m]**	**measuring interval**	**Calibration**
F2New	2009-2010	1	1774 *P*	10 min	CTD cast 2010
F2New	2010-2011	1	1778 *P*	10 min	CTD cast 2011
F2New	2011-2012	2	1420 *P*, 1770 *P*	10 min	CTD cast 2012
UK1	2007-2009	1	1980 *P*	10 min	factory 2006
UK1	2009-2010	1	1974 *P*	10 min	CTD cast 2010
UK1	2010-2011	1	1978 *P*	10 min	CTD cast 2011
UK1	2011-2012	2	1623 *P*, 1973 *P*	10 min	CTD cast 2012
G1	2009-2010	3	1812 *P*, 1966 2149	10 min 20 min	CTD cast 2009 and 2010
G1	2010-2011	3	1815 *P*, 1968 *P* 2152	20 min 20 min	CTD cast 2011
G1	2011-2012	3	1820 *P*, 1972 2170	10 min 10 min	CTD cast 2011 and 2012
UK2	2007-2009	1	2355 *P*	10 min	factory 2006
UK2	2009-2010	1	2348 *P*	10 min	CTD cast 2010
UK2	2010-2011	1	2360 *P*	10 min	CTD cast 2011
UK2	2011-2012	2	2003 *P*, 2355 *P*	10 min	CTD cast 2012
DS1	2007-2008	1	655 *P*	10 min	factory
DS1	2009-2010	1	655 *P*	10 min	CTD cast 2009
DS1	2010-2011	1	655 *P*	10 min	factory 2005
DS1	2011-2012	1	660 *P*	20 min	factory 2005
DS2	2007-2008	1	570 *P*	10 min	factory
DS2	2008-2009	1	570 *P*	10 min	factory 2005
DS2	2009-2010	1	570 *P*	10 min	CTD cast 2009
DS2	2011-2012	1	574 *P*	10 min	CTD cast 2012

The drift-rate of the sensors can be up to $0.002°C$ per year for temperature and 0.0015 psu per year for salinity. The difference between MicroCAT measurements and CTD measurements at the calibration casts were $< 0.005°C$ for temperature and for salinity < 0.005 psu. For MicroCAT measurements without calibration casts the same drift is supposed and therefore it is possible to use the factory calibrated data in addition for this thesis. However, the error of the factory calibrated MicroCAT measurements is probably higher than the measurements calibrated by CTD casts. Table 2 shows in detail which data are calibrated with CTD data and the location of the instruments in the water column. For salinity calibration the pressure plays an important role. Some MicroCATs were not equipped with a pressure sensor (see Table 2). For the calculation of salinity from conductivity and the calibration of these MicroCATs, the pressure has to be inferred from the last MicroCAT with pressure sensor at the same mooring. The exact depth of the MicroCAT is unknown, as well as the variability in depth. During the calibration, a change in pressure of approximately 30 m creates a change in the mean salinity of up to 0.01 psu. The variability of a time series is not influenced by this offset. Hence, the error of the salinity time series from MicroCATs without pressure sensor is potentially higher.

The Ammassalik moorings were partly equipped with more than one MicroCAT per mooring. The mooring equipments changed over the years, but at all moorings a MicroCAT close to the bottom (approximately 20 m above bottom) was present in every year. The DSOW is located at the bottom, hence, the data are not influenced by other water masses due to a varying DSOW plume thickness. Thus, just measurements of the MicroCATs close to the bottom are analyzed in more detail.

In this thesis, time series of potential temperature and salinity are analyzed. The first processing step after calibration is to remove outliers from the time series. Therefore every single data point is compared with the neighboring data points. Differences higher than the double standard deviation between a single data point and its neighbors are removed. The salinity is calculated from measured conductivity, temperature and pressure. The potential temperature is calculated from temperature, salinity and pressure related to the surface. Additionally, the potential density anomaly is calculated relative to the surface. Less than 0.2% of the DS1 data and less than 0.03% of the UK2 date are identified as measured outside the DSOW and are removed from the time series. All other moorings

were measuring DSOW in the whole time period. No significant tidal signals are found, thus no tidal correction is necessary. Finally, the time series were averaged to 1-day means to remove high frequency signals, and further, to reduce errors.

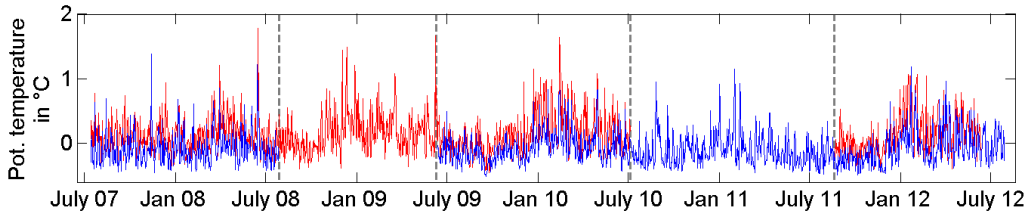

Figure 11: *Time series of potential temperature measured by MicroCATs at the Denmark Strait moorings DS1 in 650 m depth (blue) and DS2 in 570 m depth (red) between 2007 and 2012. The grey lines mark exchanges of the moorings.*

Figure 11 shows the Denmark Strait time series for the years 2007-2012. The potential temperature measured at the DS1 mooring is lower than the one measured at the DS2 mooring. This is a result of the deeper location of the mooring DS1. The same can be seen for the potential temperature time series measured at the Ammassalik array (Figure 12). Here, the temperatures are higher at the shallower moorings than at the deep UK2 mooring.

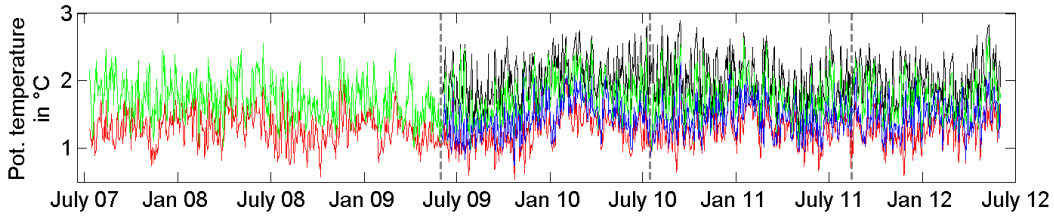

Figure 12: *Time series of potential temperature measured by MicroCATs at the Ammassalik moorings G1 in 2150 m depth (blue), UK1 in 1970 m depth (green), UK2 in 2350 m depth (red) and F2New in 1775m depth (black) between 2007 and 2012. The grey lines mark exchanges of the moorings.*

For salinity at the Denmark Strait moorings an offset can be identified in the measuring periods 2007-2008 and 2011-2012 (Figure 13). In the period 2007-2008, the salinity

measurements at the mooring DS1 is approximately $0.03 - 0.04$ *psu* lower than the measurement at DS2. Between 2009 and 2010, the time series overlap, no offset can be identified in this period. Between 2011 and 2012, the salinity measurement of DS2 is slightly higher than the one of DS1 (approximately 0.005 *psu*). Between recovery and deployment no discontinuities in any times series are obvious. Hence, the time series are of good quality.

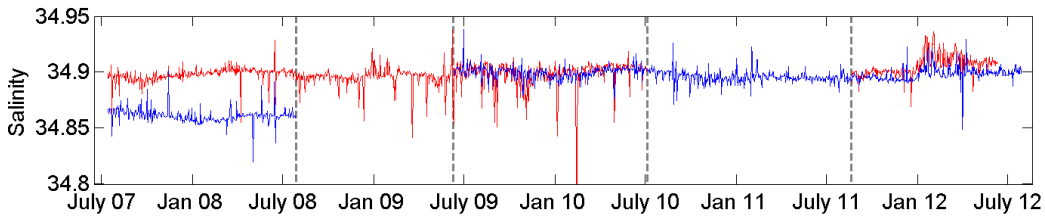

Figure 13: *Time series of salinity measured by MicroCATs at the Denmark Strait moorings DS1 in 650 m depth (blue) and DS2 in 570 m depth (red). The grey lines mark exchanges of the moorings.*

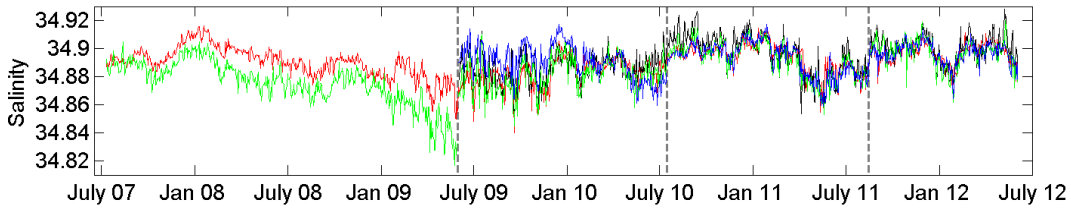

Figure 14: *Time series of salinity obtained from MicroCATs at the Ammassalik moorings G1 in 2150 m depth (blue), UK1 in 1970 m depth (green), UK2 in 2350 m depth (red) and F2New in 1775m depth (black). The grey lines mark exchanges of the moorings.*

For the salinity time series of the Ammassalik moorings a few discontinuities in the times series as well as some kind of offset (Figure 14) is found. Between July 2010 and July 2011 all salinity time series show nearly the same variability. Between July 2009 and July 2010, the salinity time series of the moorings UK1 and UK2 show nearly the same variability (Figure 14), but the time series of the mooring G1 shows higher salinities in

the first part of the deployment period and lower salinities in the 14-day mean at the end of the deployment period as the UK time series. There is also an offset between the last data before recovery in 2010 and the first data measured after the deployment two days later. In 2009 G1 could not be recovered, so there are just data from the moorings UK1 and UK2 available. The time series of UK2 shows no sudden shifts of salinity between the recoveries and deployments and seems therefore to be a good record of the DSOW between 2007 and 2012. The time series of UK1 between 2007 and 2009 shows a good comparison with the UK2 data in the first days after deployment. But after a few days salinity decreases compared to the UK2 data. In the end of the deployment period the salinities are 0.055 *psu* less than at the deployment. Between recovery and deployment in July 2009 is a large offset between the 14-day mean of the last measurements before the recovery and the 14-day mean of the first measurements after deployment. Due to the fact that no CTD calibration casts were made in 2009, the UK1 salinity measurement can not be trusted. Also the G1 near-bottom measurement between 2009 and 2010 has to be tested more precisely. A quality control is done to show if these time series have to be excluded from further analysis.

2.3 Quality control

Figure 15 shows the difference in potential temperature of the Denmark Strait moorings. In the years 2008-2009 and 2010-2011 only one MicroCAT was recovered, so there is no comparison possible. The remaining years show a higher temperature at the shallower DS2 mooring as seen in Figure 11 before. No discontinuities in any times series are obvious, hence, the time series are of good quality.

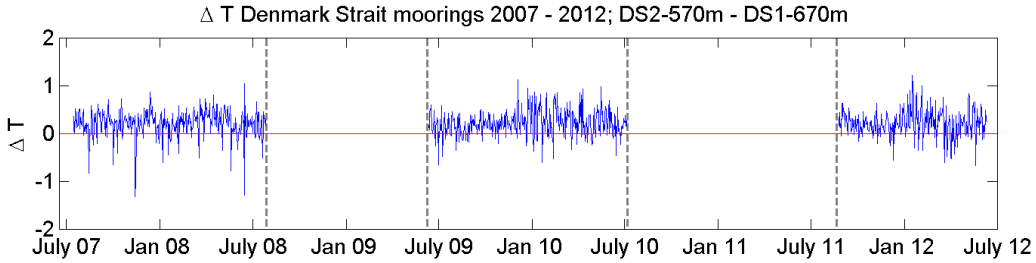

Figure 15: *Difference in potential temperature between the moorings DS1 and DS2. The red line marks the zero-difference line. The grey lines mark exchanges of the moorings.*

Figure 16 shows the difference in potential temperature of all compared time series at the Ammassalik array. The red line indicates a difference of zero. The potential temperature of F2New minus the one measured at UK2 is shown in the top of Figure 16. The potential temperature at the shallow F2New mooring is higher than at the deepest mooring UK2 as seen before in Figure 12. The annual mean difference of the time series is nearly the same over all five years of measurements. The same is valid for the calculation of the differences of G1 minus UK2 and UK1 minus UK2 (Figure 16). All measurements for potential temperature seem to be good records for the DSOW.

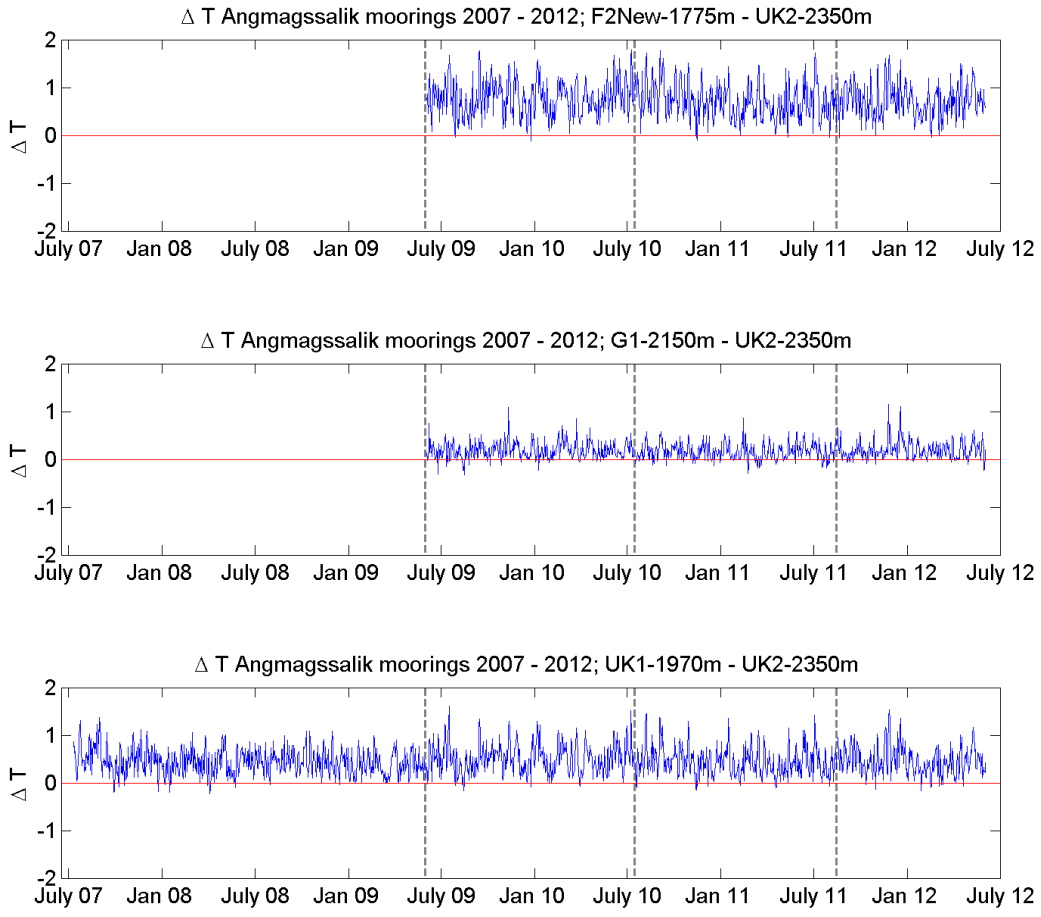

Figure 16: *Difference in potential temperature between the moorings F2New, G1, UK1 and UK2. The red line marks the zero-difference line. The grey lines mark exchanges of the moorings.*

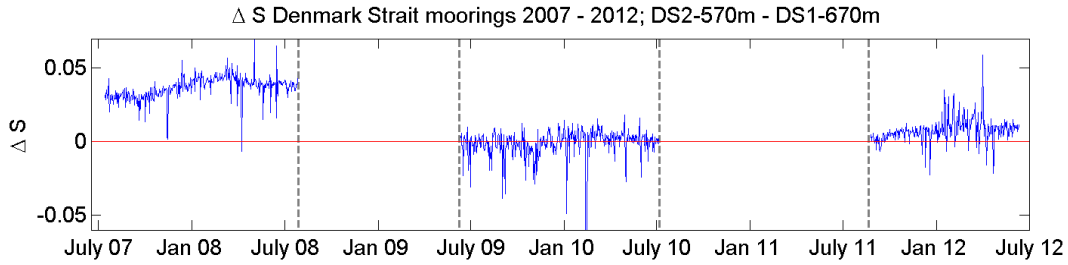

Figure 17: *Difference in salinity between the moorings DS1 and DS2. The red line marks the zero-difference line. The grey lines mark exchanges of the moorings.*

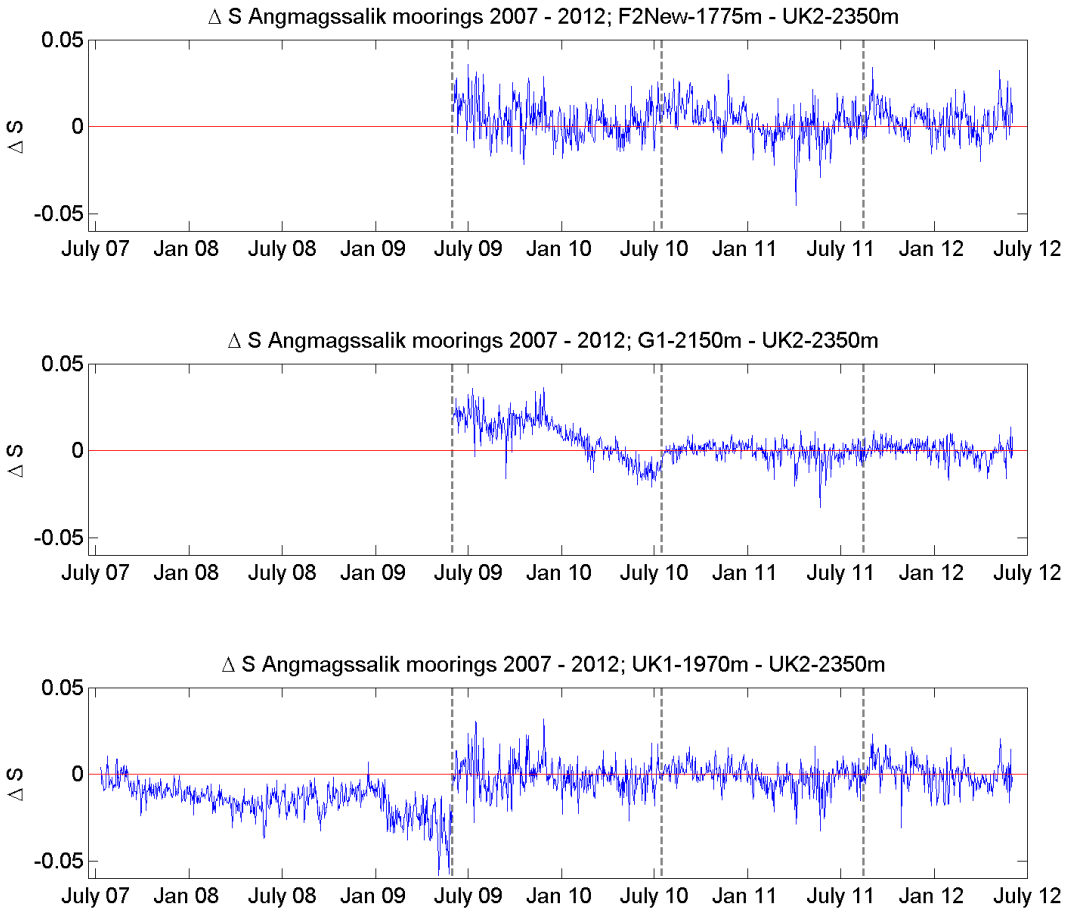

Figure 18: *Difference in salinity between the moorings F2New, G1, UK1 and UK2. The red line marks the zero-difference line. The grey lines mark exchanges of the moorings.*

By calculating the difference between the measured salinities (Figure 17 and 18), we can

now show clearly that the measurements of DS1 2007-2008, DS2 2011-2012, UK1 2007 to 2009 and G1 2009 to 2010 are different to the rest of the measurements. For the Denmark Strait measurements in the period between July 2009 and 2010 the mean difference in salinity between all time series varies around zero. The salinity measurement of the DS2 mooring between 2011 and 2012 is slightly higher, but within the instrument error. The DS1 salinity measurement between 2007 and 2008 has a large offset. This can be an effect of the missing calibration because no calibration cast is available.

For the Ammassalik moorings in the measurement period between July 2010 and 2011 the mean difference in salinity between all time series varies around zero. The same can be seen for the difference between the UK1 and UK2 measurement between 2009 and 2010. For the G1 near-bottom measurement an increase for the difference in salinity of G1 minus UK2 (and the other way around for UK1 minus G1) can be detected. This reflects the trend in the time series. The UK1 measurement between 2007 and 2009 shows also a negative trend compared to the measurements of UK2. The difference in salinity between the beginning and the end of the measurement in this period is $-0.05\ psu$.

To figure out possible causes of these offsets and trends, a closer look into the data is done but the problem can not be resolved within this master thesis. Old MicroCAT data can help to solve the problems resulting from instrument errors, a drift within the conductivity cell, biofouling or maybe other reasons. Thus, the salinity time series of the DS1 2007-2008 measurement, the G1 2009-2010 near-bottom measurement and the UK1 2007-2009 measurement are excluded from further analysis in this thesis.

Also the potential density time series are shortened, because a change in salinity of $0.01\ psu$ leads to a change in potential density of approximately $0.008\ kg/m^3$. For an possible error of $0.03 - 0.04\ psu$ this would cause an error in potential density of $\pm 0.02 - 0.03\ kg/m^3$. By calculating the potential temperature from measured temperature, pressure and salinity a change of $0.1\ psu$ in salinity leads to an change of approximately $\pm 0.0004°C$ in potential temperature. This is less than the measurement error of the temperature sensor. Therefore, the potential temperature for these periods were calculated by assuming a mean salinity.

2.4 Methods

2.4.1 Spectral analysis

In all time series we find an overlap of different frequencies of variability which often makes them difficult to understand. The spectral analysis partitions the variance of a time series as a function of frequency. After Emery and Thomson (2004) part of the spectral analysis is the Fourier analysis which allows to transform the time series from time domain into frequency domain. The Fourier transform is given by

$$Y(f) = \int_{-\infty}^{\infty} y(t) e^{-i2\pi ft} dt \tag{1}$$

with the frequency f and the time t. It can be used for all continuous and infinite functions in time domain. The time series used for this thesis are not infinite and continuous. In reality measurements are ending after a certain time. Also measurements are made with different sampling intervals. For these time series the discrete Fourier transform (DFT)

$$Y(f) = \int_{-\infty}^{\infty} \left[\sum_{k=-\infty}^{\infty} y(t)\delta(t - n\Delta t)\Delta t \right] e^{-2\pi ft} dt \tag{2}$$

with the continuous sampling rate n and the discrete sampling rate Δt of the signal is used. The limiting factor to discern oscillations is given by the frequency resolution

$$\Delta f = f_{min} = \frac{1}{T} = \frac{1}{n_{max}\Delta t} \tag{3}$$

where $T = n_{max}\Delta t$ is the length of the time series and f_{min} is the smallest frequency which can be detected. The maximum frequency which can be detected is the Nyquist frequency

$$f_N = \frac{1}{2\Delta t}. \tag{4}$$

For partitioning the variance, the power spectral density (PSD) is used. The PSD points out the frequencies which are dominant in the time series and can be calculated by

$$E = \int_{-\infty}^{\infty} |y(t)|^2 dt. \tag{5}$$

The time series used for this thesis are cut after certain time because of mooring recovery. To analyze them they are considered to be the product of an infinitely long time series with a rectangular window which spans the duration of the measured data. So, the discrete spectrum is a convolution of the real spectrum. For further analyses the *wavelet* spectrum is calculated. After Torrence and Compo (1998) the *wavelet* analysis localizes the non stationary power at different frequencies. The *wavelet* spectrum is blind to deterministic trends. Another benefit is that it determines the time when the dominant modes of variability occur by decomposing the time series with the *wavelet* transform. It is based on the *wavelet* function $\Psi_0(\eta)$, depending on a non dimensional "time" parameter η. The *wavelet* function can be chosen individually. For the analysis of the mooring time series the *wavelet* basis *Morlet* is used because it is a non orthogonal and complex *wavelet*. Because the time series is non stationary, one expects a continuous variation in the *wavelet* amplitude, which can be dissolved by a non orthogonal *wavelet*. The *wavelet* has to be complex due to the oscillatory behavior of the time series. The *Morlet wavelet* consists of a plane wave modulated by a Gaussian distribution:

$$\Psi_0(\eta) = \pi^{-1/4} e^{i\omega_0 \eta} e^{-\eta^2/2}. \tag{6}$$

ω_0 is the non dimensional frequency which can be varied. The corresponding *wavelet* transform to the *wavelet* function is given by

$$W_n(s) = \sum_{n'=0}^{N-1} x_{n'} \Psi^* \left[\frac{(n-n')\delta t}{s} \right]. \tag{7}$$

The (*) indicates the complex conjugate, the Ψ is the normalized Ψ_0.
The *wavelet* transform $W_n(s)$ is complex due to the fact that the *wavelet* function $\Psi(\eta)$ is complex. Hence, the transform can be divided into a real and an imaginary part. Finally, the *wavelet power spectrum* can be defined as $|W_n(s)|^2$.
Before calculating the *wavelet* transform it is important to set the scale s in Equation 7 correctly. It is practical to set the scale as a fractional power of two:

$$s_j = s_0 2^{j\delta j}, \tag{8}$$

with $j = 0, 1, ..., J$ and

$$J = \delta j^{-1} log_2(N\delta t / s_0), \tag{9}$$

where J determines the largest scale and s_0 is the smallest resolvable scale which should be chosen as approximately $2\delta t$. δj depends on the chosen wavelet function. The largest value for δj is 0.5 for the *Morlet wavelet* (Torrence and Compo, 1998). A smaller δj gives a finer resolution but with an increasing scale, the resolution in time decreases, which makes it more difficult to localize an amplitude in time.
In the end it is important to calculate a 95% significance level to indicate edge-effects which distort the result. Therefore, a background Fourier power spectrum is assumed. The result is a wavelet power spectrum where the significance level, calculated by assuming red noise, point out the dominant frequencies of the spectrum. Together with the power spectrum calculated from the Fourier transformation before, it is now possible to define the dominant frequencies, as well as the times when they occur.

2.4.2 Harmonic Analysis

The analyzed time series in this thesis are at most five years long. To detect signals with a period exceeding one-third of a year the wavelet analysis is too much influenced by occurring edge effects. Hence, a harmonic analysis is used to identify a seasonal cycle.

The harmonic analysis is based on the least-square technique to solve for constituents of a specified frequency, like the seasonal frequency. After Emery and Thomson (2004) it yields the required amplitude and phase lag of the seasonal cycle coefficients. These coefficients can be used to reconstruct the seasonal cycle fitting to the original time series.

The amplitude and phase of the seasonal cycle is estimated by minimizing the squared difference - the least square - between the original time series and the fit to that series. The coefficients are found through a solution $(M+1) \times (M+1))$ matrix equation, where M is the number of resolvable constituents. The time series $x(t_n)$, with $n = 1, ..., N$ can be expanded for possible harmonic constituents to

$$x(t_n) = \bar{x} + \sum_{q=1}^{M} [A_q \ \cos(2\pi f_q t_n) + B_q \ \sin(2\pi f_q t_n)] + x_r(t_n) \tag{10}$$

with the mean value $\bar{x}$ of the time series, the constant frequency f_q and x_r the residual portion of time series. The amplitude can be calculated as

$$C_q = (A_q^2 + B_q^2)^{1/2} \tag{11}$$

and the phase lag as

$$\Phi_q = \tan^{-1}(B_q/A_q) \tag{12}$$

The mean value $\bar{x}$ should be subtracted from the original time series before computation of the coefficients to reduce roundoff errors.

2.4.3 Filter

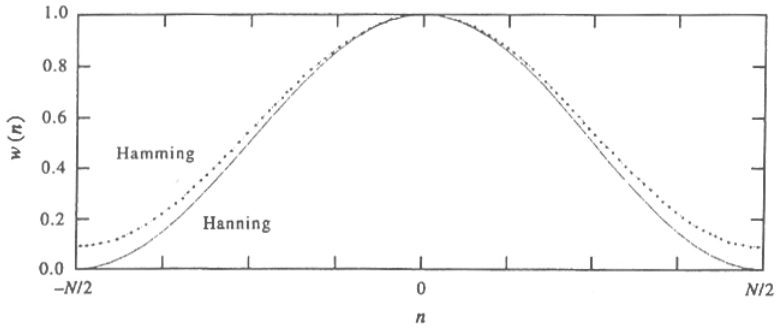

Figure 19: *Example for a Hanning and Hamming window for $N = 41$ $(-20 \leq n \leq 20)$ from Emery and Thomson (2004).*

The mooring data used for this thesis show high variability on small time scales. This makes it difficult to compare long term signals within the Denmark Strait data to those at Ammassalik because they are overlain. To remove the variability on short time scales a low-pass filter is used. After Emery and Thomson (2004) the ideal low-pass filter has to satisfy the following relations:

$$|H(\omega)| = 1 \; for \; |\omega| \leq \omega_c \tag{13}$$

$$|H(\omega)| = 0 \; for \; \omega_c \leq \omega \tag{14}$$

where ω_c is the cut-off frequency. The low pass filter lets through low-frequency signals but damps high-frequency signals. In this thesis, a low-pass Hamming window is used.

The Hamming window is defined as

$$\omega(n\delta t) = 0.54 + 0.46cos(2\pi n/N) \tag{15}$$

with $n = -N/2, ..., N/2$, where N is the number of values of the time series. The Hamming window has a spectral distribution similar to a Hanning window, but has more "efficient" side-lobe attenuation as seen in Figure 19. After using the low-pass filter it is now possible to determine long time variability signals and compare the signals found at the different moorings.

2.4.4 Correlation

To investigate the effect of entrainment on the variability of the DSOW between the Denmark Strait sill and Ammassalik, the time series are correlated. A good correlation of the time series indicates an advection of the signals from the Denmark Strait to the Ammassalik array. No correlation of the time series indicates that entrainment destroys signals before they reach the Ammassalik array. It is important to remember that the Denmark Strait Overflow Water needs between 9 and 50 days from the Denmark Strait array to the Ammassalik array (Dickson et al., 2008).

After Schönwiese (2006) the cross-correlation is used for the analysis of two different time series which are shifted. The cross-correlation-coefficient is given by

$$r_C = \frac{\sum_{i=1}^{n-\tau} a_i' b_{i+\tau}}{\sqrt{\sum_{i=1+\tau}^{n} b_i'^2 \sum_{i=1}^{n-\tau} a_i'^2}}. \tag{16}$$

$\tau = 0, 1, ..., M < n$ is the time shift between the time series from the Denmark Strait array (represented by a) and the Ammassalik array (represented by b).

$$s_C = \frac{1}{n-1-\tau} \sum_{i=1}^{n-\tau} a_i' b_{i+\tau}. \tag{17}$$

The result of the cross-correlation-coefficient has to be in the range $-1 \leq r_C \leq +1$. If the signals in the time series are in phase and perfectly correlated the cross-correlation-

coefficient is 1. If they are in antiphase and perfectly correlated the coefficient is -1. If the coefficient is 0 the time series are not correlated. It is important to test for no correlation to rate the results of the cross-correlation. The probability of getting a correlation by random chance as large as the observed, while the true correlation is zero is calculated as the value P. If P is smaller than 0.05, then the correlation is in the 95% confidence interval. If P is higher, the correlation is likely random.

2.4.5 Water mass analysis

The water mass analysis is used to detect the water masses which are entrained into the Denmark Strait Overflow by the surrounding water on the way from Denmark Strait to the Ammassalik array. Because there are only salinity and temperature data available for this thesis, a simple set of equations is used to estimate the contributing water masses. This water mass analysis is also known as the "mixing triangle" explained in detail in Tomczak (1981). The following equations are used:

$$T_{obs} = T_1 x_1 + T_2 x_2 + T_3 x_3 \tag{18}$$

$$S_{obs} = S_1 x_1 + S_2 x_2 + S_3 x_3 \tag{19}$$

$$1 = x_1 + x_2 + x_3 \tag{20}$$

where T_{obs} and S_{obs} are the observed values at the Ammassalik array, T_1 and S_1 describes the DSOW observed at the Denmark Strait sill, T_2 and S_2 describes the Atlantic Water and T_3 and S_3 describes another water mass (e.g. LSW or EGC water) which is entrained into the Plume on the way south. Equation 20 is the mass conservation equation. With this set of equations the amount (x) of every source water mass contributing to the measured temperature and salinity properties can be determined. For a mixing of more than three water masses additional information about the water mass characteristics have to be known, like oxygen, phosphate or nitrate concentrations. With these additional tracers an optimum multi parameter analysis can be done. For the DSOW measured at the Denmark Strait and Ammassalik between 2007 and 2012 no tracer data are available during the work on this thesis. Hence, the simple mixing triangle analysis is used.

3 Variability of the DSOW 2007 - 2012

This chapter describes the DSOW variability between 2007 and 2012. First, the power spectra are shown and described and the need for filtering is explained. Afterwards, the 20 day low-pass time series are shown. The variability is described on the basis of the calculated power spectra.

3.1 Wavelet spectra

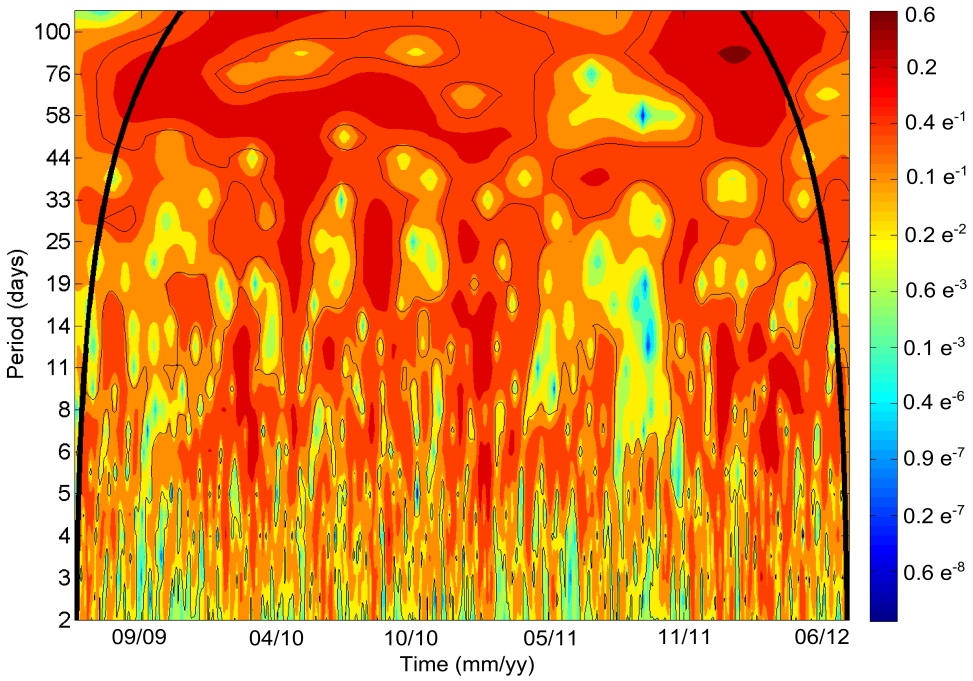

Figure 20: *Wavelet spectrum for potential temperature time series of the Denmark Strait mooring DS1 in the time period 2009-2012. Outside the thick black lines edge effects occur. The thin black lines indicate the 95% confidence interval. The colors indicate the energy in* $^{\circ}C^2$.

The wavelet analysis localizes the non stationary power at different frequencies. It gives an overview about the periods found in the time series and points out when they occurred. It also shows the value of power for the periods.

Figure 20 shows the significant periods (red colored between the thin black lines) of the time series measured at DS1 between 2009 and 2012. Periods of 2-10 days occur nearly every month between 2009 and 2012. Red color marks high energy. These repeating signals are eddies which have a period of 2-10 days and are described more precisely in the work of Voet and Quadfasel (2010) and Moritz (2011). Also significant periods of 10-20 days can be identified. These periods are often found in oceanic research but the source could not be discovered yet (Friedrichs, 2011). Highest significant energies can be identified within periods of 20 to 100 days. These can not be seen in the daily mean time series because they are overlain by the high variability on shorter time scale.

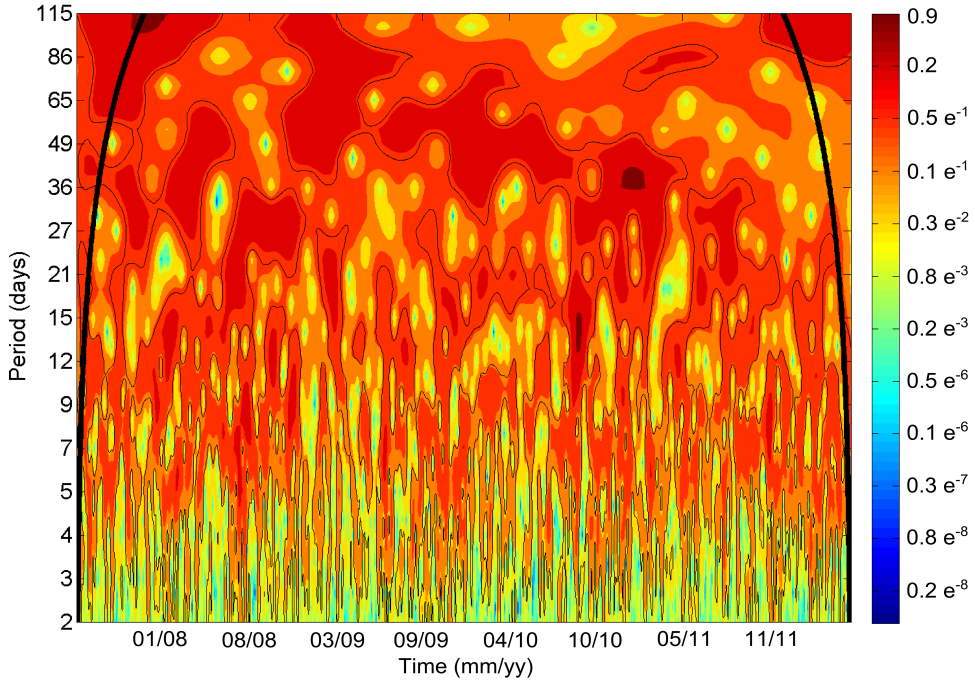

Figure 21: *Wavelet spectrum for potential temperature measured at the Ammassalik mooring UK2 in the time period 2007-2012. Outside the thick black lines edge effects occur. The thin black lines indicate the 95% confidence interval. The colors indicate the energy in* $^{\circ}C^2$.

Similar structures can be seen in the measurements at the Ammassalik array (Figure 21). Repeating periods of 2-10 days can be clearly identified. These are eddies which occur regularly at the DSOW plume and cause horizontal entrainment of ambient water into

the plume (Voet and Quadfasel, 2010). In contrast to the Denmark Strait time series periods of 10 to 20 days occur more often and more regular. The highest energies can also be found in periods of 20-100 days as seen before in the Denmark Strait.

The spectral analysis for all Denmark Strait moorings shows similar results in the wavelet plots, as the spectra of all Ammassalik measurements. Thus just the deepest moorings of both arrays, DS1 and UK2, are shown and described.

The variance in salinity is much smaller than in potential temperature. Significant periods can be found in the 2-10 day period band but with low energy ($E < 10^{-8}\ psu^2$). Also significant periods can be found in the 20-100 day period band but also with highest energies of $10^{-4}\ psu^2$. Therefore only the spectral analysis for the potential temperature time series are shown and discussed in more detail.

Within the wavelet plots it is not possible to detect a seasonal cycle because edge effects occur within the wavelet analysis. Longer periods can also not be detected because the time series are to short. To detect the seasonal cycle a harmonic analysis is done.

3.2 Seasonal cycle

The seasonal cycles are calculated with a harmonic analysis. Figure 22 shows the seasonal cycle for the DS1 mooring. In both Denmark Strait moorings a seasonal cycle can be detected in potential temperature and salinity. Amplitudes of the seasonal cycle are $0.12°C$ - $0.13°C$ for potential temperature with a maximum in March and minimum in September. For salinity amplitudes are $0.002\ psu$ with a maximum in April and a minimum in October. The detected seasonal cycle can explain 9-10% of the variance in potential temperature and 4-5% of the variance in salinity for the period 2007 to 2012. The seasonal cycle of DS2 is shown in Figure 36 in the appendix. Jochumsen et al. (2012) found that the detected seasonal cycle at the Denmark Strait can explain less than 5% of the variance in a time period of more than 10 years.

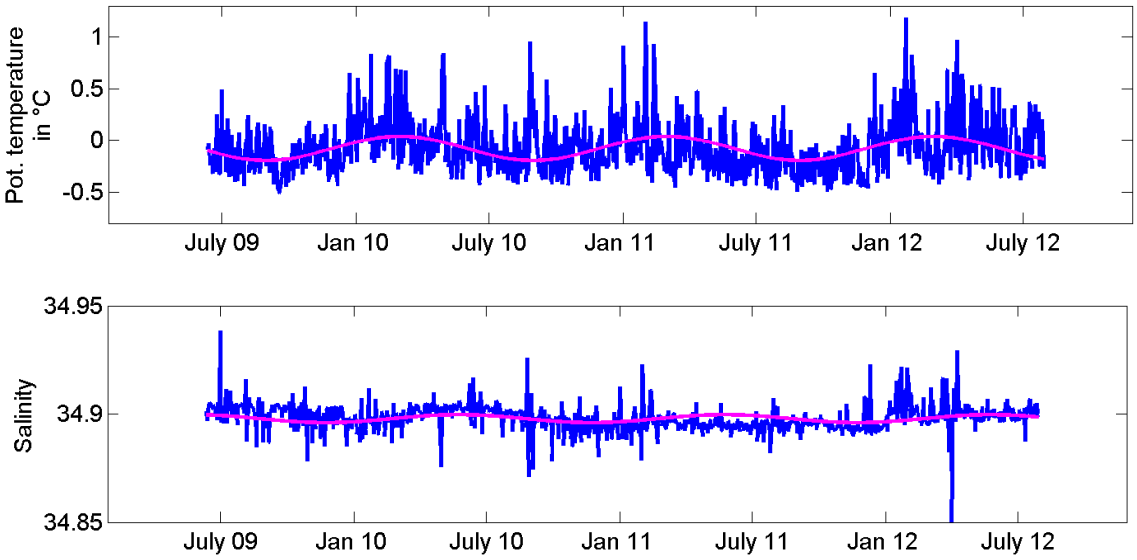

Figure 22: *Seasonal cycle (magenta) at DS1 for potential temperature (top) and salinity (bottom). The daily mean time series are shown in blue.*

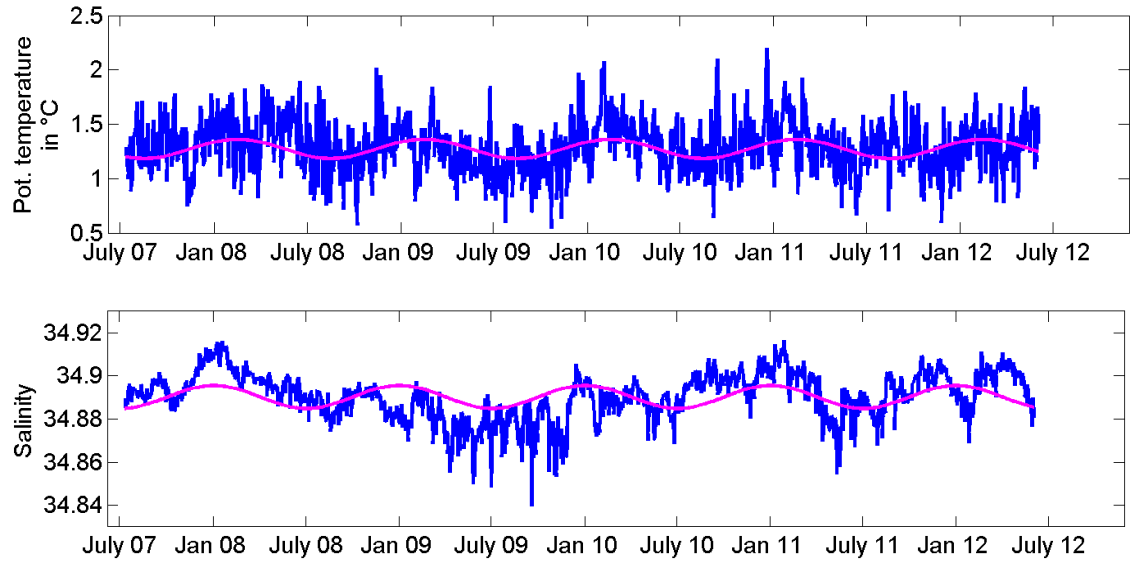

Figure 23: *Seasonal cycle (magenta) at UK2 for potential temperature (top) and salinity (bottom). The daily mean time series are shown in blue.*

Figure 23 shows the seasonal cycle at the UK2 mooring. The seasonal cycle can also be detected at the other Ammassalik moorings. The amplitudes are higher at the deeper G1

and UK2 mooring than at F2New and UK1. For potential temperature, the maximum amplitude is $0.11°C$ with a maximum in March and a minimum in September as seen in the Denmark Strait moorings before. For salinity, the maximum amplitude is 0.008 *psu* with a maximum in December/January and a minimum in June/July. While the seasonal cycles of the potential temperature are in phase, the seasonal cycles in salinity show a phase shift of eight month between the mooring locations. The detected seasonal cycle can explain up to 10% of the variance in potential temperature (less at the shallower moorings) and up to 11% of the variance in the salinity. For longer periods these numbers seem to reduce as seen in the Denmark Strait data. However, the seasonal cycle can just explain a very small part of the variance. To make the other long periods visible and analyzable, the time series have to be filtered to exclude the high variability on short time scales. Therefore a 20 day low pass filter is applied to remove the high frequency variability.

3.3 20 day low pass filtered time series

The wavelet plots in Chapter 3.1 show a minimum in energy at a period of 20 days. Thus, an 20 day low pass filter is applied to remove the frequencies on short time scales. The 20 day low pass filtered time series from Denmark Strait are shown in Figure 24. The mean values and standard deviations for the 20 day low pass filtered time series are shown in Table 3.

Table 3: *Mean values and standard deviations of potential temperature, salinity and potential density anomaly of the MicroCATs measurements between 2007 and 2012 at the Ammassalik array*

	mean $\theta[°C]$	mean S	mean $\sigma_\theta[kg/m^3]$
DS1	-0.08 ± 0.13	34.898 ± 0.003	28.03 ± 0.01
DS2	0.15 ± 0.17	34.899 ± 0.006	28.02 ± 0.01
F2New	2.00 ± 0.17	34.894 ± 0.011	27.89 ± 0.01
UK1	1.74 ± 0.16	34.889 ± 0.011	27.9 ± 0.01
G1	1.45 ± 0.15	34.894 ± 0.009	27.93 ± 0.01
UK2	1.27 ± 0.14	34.890 ± 0.010	27.94 ± 0.01

The Denmark Strait values agree with the published data from Jochumsen et al. (2012)

for the time period 2005-2011. In the DS potential temperature time series, no extreme events are obvious. Both moorings show similar signals in potential temperature, salinity and in the potential density anomaly. The shallower DS2 mooring measured freshening events up to 0.02 *psu* occurring on time scales of up to two month. These freshening events were not measured at the deeper DS1 mooring. The different variability could therefore be a result of a shift of the DSOW plume at the shelf for certain periods. The DS2 mooring then would not be in the deep mixed layer of the DSOW, and thus, be measuring in the stratified layers or in the low salinity lid. The lower densities in this time period prove this theory. In all Denmark Strait time series no trend is found in the period 2007 to 2012.

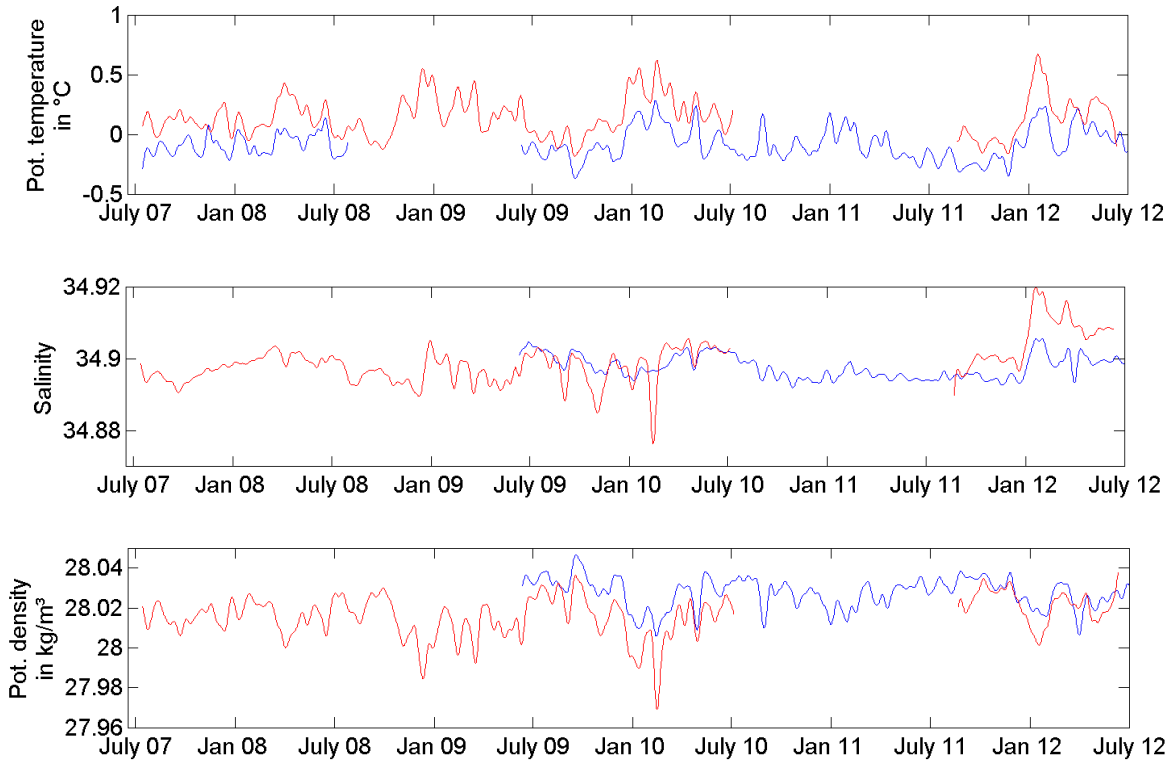

Figure 24: *20 day low pass filtered time series of potential temperature (top), salinity (middle) and potential density anomaly (bottom) of the DSOW at the moorings DS1 (blue) and DS2 (red) between 2007 and 2012.*

The 20 day low pass filtered time series measured at the Ammassalik array are shown in Figure 25. The mean values and standard deviations for the 20 day low pass filtered time

series are shown in Table 3. In all Ammassalik time series no trend is found in the period 2007 to 2012.

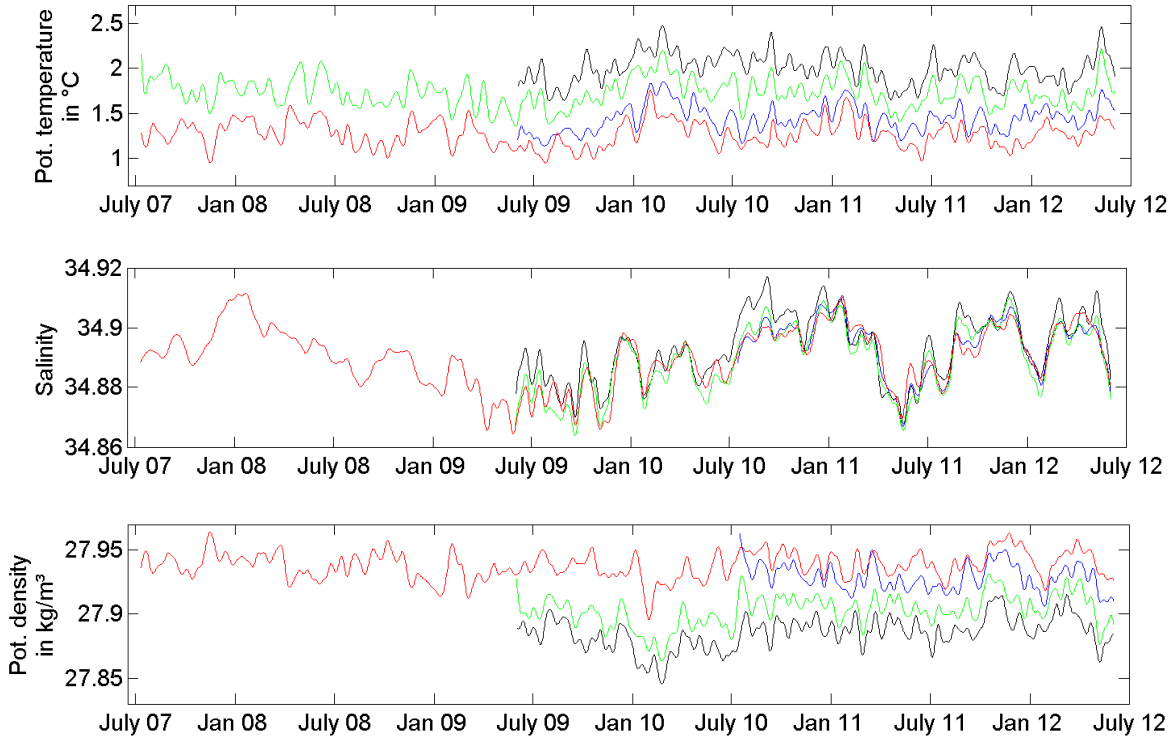

Figure 25: *20 day low pass filtered time series of potential temperature (top), salinity (middle) and potential density anomaly (bottom) of the DSOW at the moorings F2New (black), G1 in 2150 m depth (blue), UK1 (green) and UK2 (red) between 2007 and 2012.*

In the potential temperature time series no outstanding events are obvious. All moorings show similar signals in potential temperature, salinity and in the potential density anomaly. The long term variability of the salinity time series at Ammassalik is larger than seen at Denmark Strait. The freshening events measured at DS2 in 2009 to 2010 can not be found at the Ammassalik moorings. Between January 2008 and December 2010 a local salinity minimum was found. This could be part of a multi-year cycle. After December 2010 the salinity seems to remain at the same level except of two freshening events. The first freshening event can be identified in the period April to June 2011 with magnitude in salinity up to 0.023 *psu*. In January 2012 the next freshening event with a magnitude up to 0.026 *psu* occurs within one month. These freshening events have approximately

half the magnitude of the extreme freshening events found in 1999 and 2004, which had a magnitude of $0.04 - 0.06$ *psu* (Hall et al., 2011).

3.4 Spectra of the 20 day low pass filtered data

Figure 26 shows the wavelet spectrum (top) and power spectrum (bottom) for potential temperature at the Denmark Strait mooring DS1 between 2009 and 2012. The spectra at DS2 show similar significant periods and frequencies. In the Denmark Strait potential temperature data no dominant periods or frequencies are evident. Period bands, which occur almost over the whole measuring period, can be detected between periods of 42 to 120 days. Bands of periods between 30 and 40 days occur frequently, just cut off in autumn every year, as well as partly in spring. Bands of periods between 20 and 30 days are present in January, April and August 2010, January, April and November 2011, and April 2012. These bands do not occur regularly. To prove this, longer time series are needed.

Figure 27 shows the wavelet spectrum (top) and power spectrum (bottom) for potential temperature at the Ammassalik mooring UK2 between 2007 and 2012. The spectra at the other Ammassalik moorings show similar results. In the Ammassalik potential temperature data significant periods or bands of periods can be seen but less than at the Denmark Strait. However, the significant periods have higher energies at the Ammassalik array than at the Denmark Strait. As well as in the Denmark Strait no dominant periods or frequencies are evident. The bands of periods are not regularly occurring. In February/March 2008 bands of periods between 30 and 60 days occurred. In summer 2008 bands of periods between 20 and 35 days occurred, which changed in autumn/winter to periods between 36 to 100 days. Periods between 50 and 60 days were present for 1 1/2 year (January 2009 to June 2010). The band of periods changed during this time from a range of 40-100 days to a range of 35-65 days. After summer 2010 a band of periods between 25 and 50 days was present until spring 2011. In summer 2011 this band of periods can be detected again. Between autumn 2010 and summer 2011 a band of periods between 70 and 85 days can also be detected.

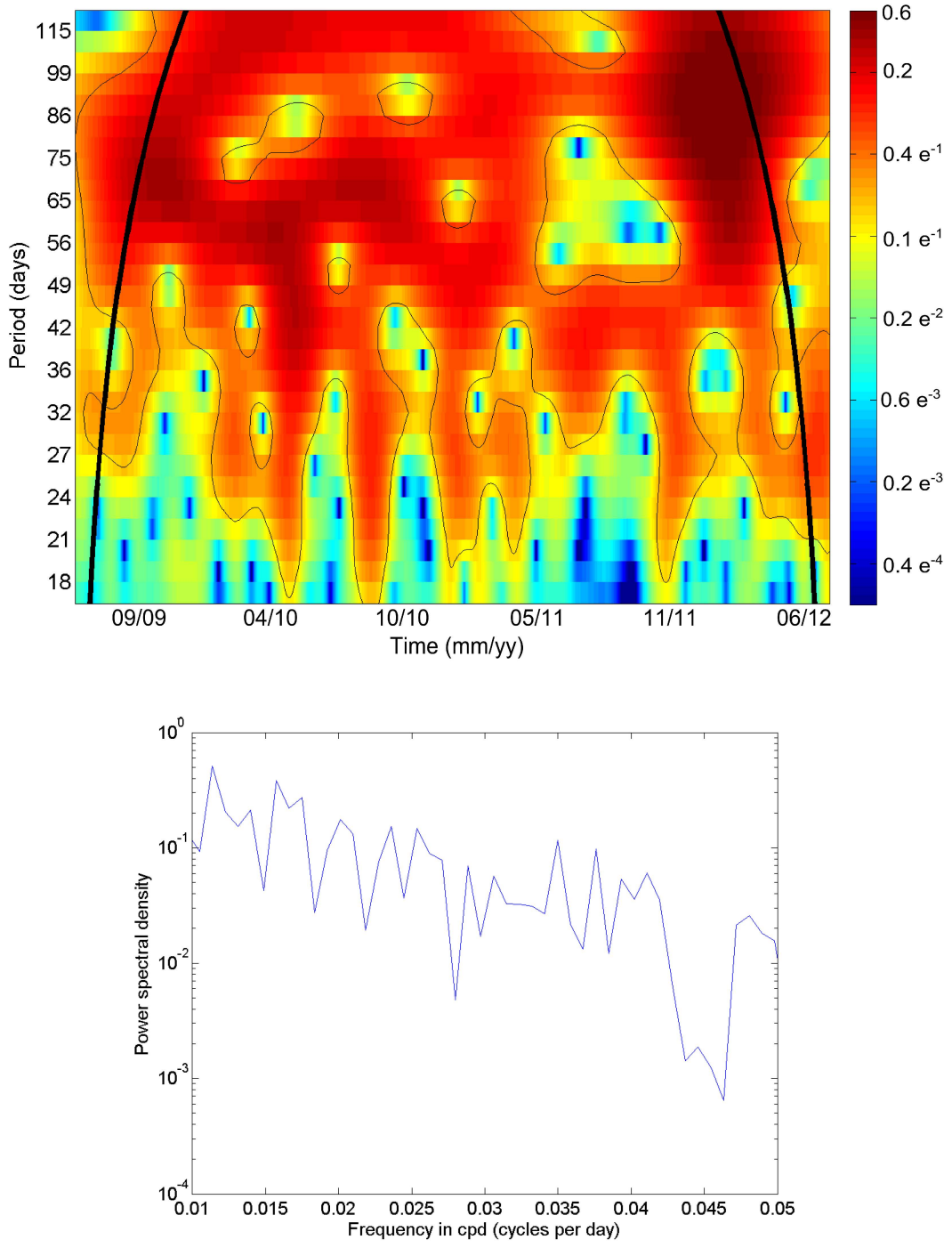

Figure 26: *Wavelet spectrum (top) for potential temperature of the 20 day low pass filtered data of the Denmark Strait mooring DS1 in the time period 2009-2012. Outside the thick black lines edge effects occur. The thin black lines indicate the 95% confidence interval. The colors indicate the energy in* $°C^2$*. The power spectrum (bottom) shows the related frequencies.*

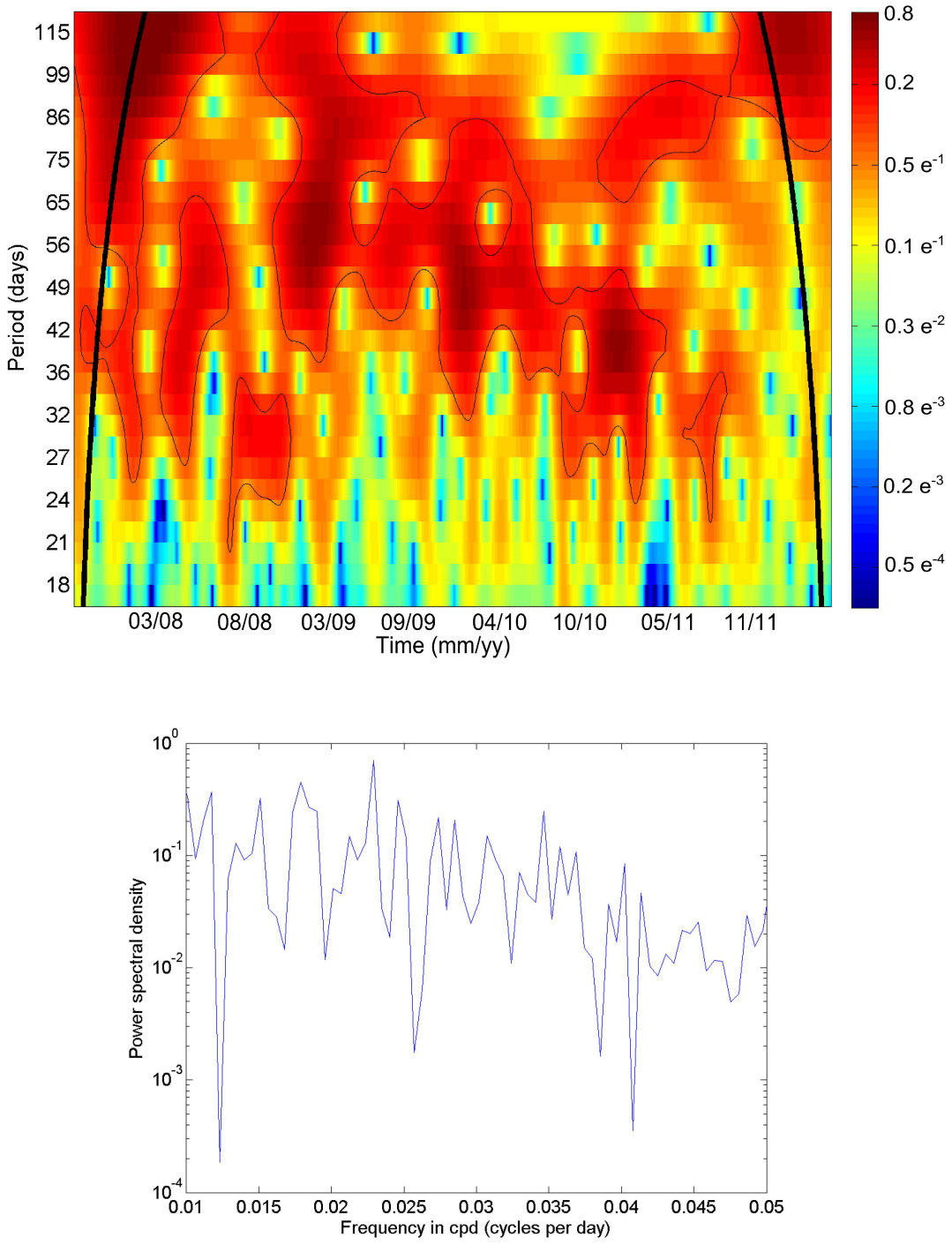

Figure 27: *Wavelet spectrum (top) for potential temperature of the 20 day low pass filtered data of the Ammassalik mooring UK2 in the time period 2007-2012. Outside the thick black lines edge effects occur. The thin black lines indicate the 95% confidence interval. The colors indicate the energy in* $°C^2$*. The power spectrum (bottom) shows the related frequencies.*

The power spectra (Figure 26 and 27) show no dominant frequencies being evident in the time period 2007 to 2012.

In a direct comparison the variability is not the same in the Denmark Strait and Ammassalik time series. To prove the similarity, the time series have to be correlated. The correlation can show whether signals within the time series are advected or if they are destroyed by entrainment. The correlations are shown and described in Chapter 4.

3.5 Summary and discussion

No trend was detected in the time series between 2007 and 2012. The annual mean salinity measured at the Denmark Strait sill in the period 2007-2012 is between 34.895 *psu* and 34.906 *psu*, which is higher than the annual mean salinity values between 1993 and 2001 (see Figure 7). Also at the Ammassalik array no trend is detected. The annual mean values are between 34.881 *psu* and 34.901 *psu*. The mean values differ at each mooring location and each year of measurement, which represents interannual variability. To prove this, longer time series are necessary.

The variance of the DSOW salinity time series at Denmark Strait is less than the variance at Ammassalik. High variability on short time scales are dominating all time series. Part of this variability is a result of crossing eddies. A seasonal cycle can be detected in all time series, but can only explain up to 10% of the variance. The other periods can not yet be associated with relevant processes in the deep ocean. In all spectra no regularly occuring dominant frequency is evident.

No extreme freshening events occurred at the Ammassalik array in the time period 2007 to the beginning of 2011. The salinity decreases between January 2008 and July 2009. It increases again between July 2009 and December 2010. In the measurement period 2011-2012, two freshening events can be identified. One occurs in April to June 2011 and the other one in January 2012. Both events are not as strong as the ones measured in 1999 and 2004 and described by Dickson et al. (2008). The magnitude is approximately half of the ones found in 1999 and 2004. For potential temperature no outstanding events can be recognized. The freshening events present in the Ammassalik time series were not seen in the Denmark Strait measurements. Further analysis has to reveal if the variability at the Denmark Strait sill, is correlated to that at Ammassalik.

4 Signal propagation

To prove if signals in potential temperature and salinity are advected between the Denmark Strait and the Ammassalik array a cross-correlation is done. All time series within the arrays are correlated to discover the variations within the DSOW plume properties at each array. Then the Denmark Strait data are correlated with the Ammassalik data. Advected signals are identified, as well as a total change of the variation of the DSOW properties between Denmark Strait and Ammassalik.

4.1 Correlations within the arrays

The variability measured at DS1 and DS2 is not always exactly the same, as seen in Chapter 3. The distance between DS1 and DS2 is about 10 km, so measurements could be influenced by a shift of the DSOW plume. The same behavior can be found at the Ammassalik array. There the distance between neighboring moorings varies between 10 to 25 km. The calculated correlation coefficient within one array gives an estimate about the variation of the DSOW inside the plume. The 20 day low pass filtered time series within one array are correlated for all possible correlation periods.

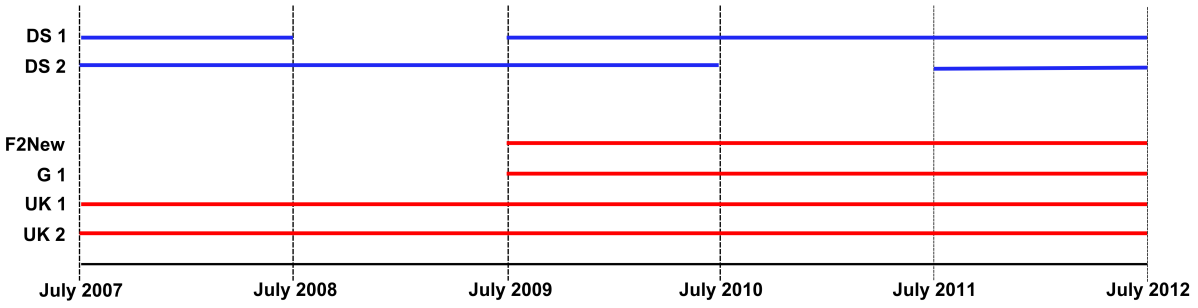

Figure 28: *Possible correlation time periods for potential temperature.*

The correlation periods are different for the different mooring combinations. The possible correlation periods for potential temperature are shown in Figure 28. For the Denmark Strait moorings three one-year periods can be correlated. For salinity the possible correlation periods differ from the ones for potential temperature (Figure 29).

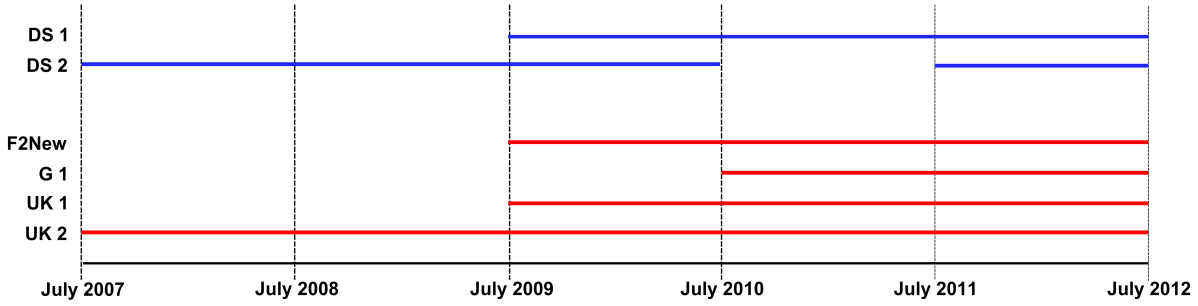

Figure 29: *Possible correlation time periods for salinity.*

The results of the significant correlations for the DS1 and DS2 mooring can be seen in Table 4. The time series of potential temperature and salinity are not showing the exact variations at DS1 and DS2 during the same measuring period. The correlation of the potential temperature is best for the period 2011-2012 with a correlation coefficient of 0.87. For salinity the highest correlation coefficient is 0.88 for the same period. This supports the assumption that the DSOW plume is shifted during some time periods, which leads to measurements of one mooring in the deep DSOW core and the other in the stratified layer.

Table 4: *Significant correlation of the 20 day low pass filtered data from DS1 and DS2*

	period		
	2007-2008	**2009-2010**	**2011-2012**
pot. temperature	0.54	0.72	0.87
salinity	-	0.53	0.88

Table 5: *Significant correlation of the 20 day low pass filtered data from Ammassalik moorings for the period 2009-2012. The G1 salinity is only correlated for the period 2010-2012.*

(a) Correlation of pot. temperature

	UK1	**G1**	**UK2**
F2New	0.88	0.56	0.47
UK1	-	0.73	0.58
G1	-	-	0.87

(b) Correlation of salinity

	UK1	**G1**	**UK2**
F2New	0.96	0.90	0.86
UK1	-	0.96	0.92
G1	-	-	0.96

The results of the significant correlations for the Ammassalik moorings can be seen in Table 5. The longest possible correlation period for almost all mooring combinations is three years long. This period is chosen to get results which are comparable among each other. For correlations of the salinity time series with G1 only a shorter time period is available. The correlation coefficient is best for neighboring moorings and decreases with distance between the mooring locations. For potential temperature the highest correlations have a coefficient between $0.73 - 0.88$ and 0.96 for salinity. To prove how the correlation coefficients change over time, correlation coefficients are calculated for every year and can be looked up in the Appendix 7.2. For potential temperature the correlation coefficient of the yearly periods is between 0.42 and 0.91. For salinity the coefficient is between 0.71 and 0.98.

The smaller correlation coefficients for potential temperature show a high temperature variability within the plume at both arrays. The salinity signals measured at the Denmark Strait sill moorings differ. The high correlation coefficients for salinity at the Ammassalik array indicate less variability of salinity within the plume after descending. This means that the plume is mostly uniform in salinity on the spatial scale (nearly 50 km) at Ammassalik. The Denmark Strait results indicate that the plume is narrower at the sill. A uniformity can not be found in the 10 km distance between the Denmark Strait moorings.

4.2 Correlations of the DSOW between the Denmark Strait and Ammassalik array

To prove if signals are advected between the Denmark Strait sill and the Ammassalik array (see Chapter 1.4), the time series from the Ammassalik array are correlated with the time series from the Denmark Strait array. For all correlations a correlation coefficient for a time lag between the Denmark Strait and Ammassalik array of 1-55 days was calculated. The highest correlation coefficient with the corresponding time lag for potential temperature of every mooring combination is shown in Table 6. The uncertainty for the time lag varies between 3 and 8 days.

Table 6: *Potential temperature correlation of the 20 day low pass filtered data from the Ammassalik moorings with the data from Denmark Strait moorings DS1 and DS2. Only significant correlation coefficients are shown.*

2007-2008	**F2New**	**UK1**	**G1**	**UK2**
DS1	-	0.38**@**21days	-	0.35**@**18days
DS2	-	0.31**@**22days	-	0.49**@**20days
2008-2009	**F2New**	**UK1**	**G1**	**UK2**
DS1	-	-	-	-
DS2	-	0.51**@**14days	-	0.72**@**15days
2009-2010	**F2New**	**UK1**	**G1**	**UK2**
DS1	0.58**@**12days	0.70**@**10days	0.69**@**16days	0.65**@**17days
DS2	0.69**@**10days	0.79**@**8days	0.70**@**32days	0.75**@**23days
2010-2011	**F2New**	**UK1**	**G1**	**UK2**
DS1	0.25**@**10days	0.44**@**12days	0.56**@**12days	0.44**@**16days
DS2	-	-	-	-
2011-2012	**F2New**	**UK1**	**G1**	**UK2**
DS1	0.24**@**28days	0.26**@**41days	0.52**@**14days	0.60**@**20days
DS2	-	-	0.52**@**11days	0.68**@**13days

The correlation coefficients for potential temperature between DS1 and the Ammassalik mooring data are between 0.24 and 0.70 for a time lag of 10-41 days. The coefficients for the correlation with the DS2 mooring data are between 0.31 and 0.79 with a time lag of 8-32 days. The correlations of the Ammassalik mooring data with the DS2 mooring data are better than with DS1 except of one correlation of UK1 and DS1 in 2007. The shallow F2New mooring data has smaller correlation coefficients than the other Ammassalik mooring data. The highest correlations can be found in the year 2009-2010 for all mooring combinations. Within this time period the best correlations are found with the UK1 data. For the correlation with DS1 the coefficient is 0.70 with a time lag of 10 days. For DS2 the correlation coefficient is 0.79 with a time lag of 8 days. In 2011-2012 the highest correlations can be found for the UK2 data within a time lag of 13-20 days. Most of the correlations can be found between 10 and 20 days time lag. Most correlation coefficients are in the range of the ones found by correlation within the arrays (Chapter

4.1). The potential temperature time series therefore show good correlations within the range of the plume variability. Thus potential temperature signals are advected from the Denmark Strait to the Ammassalik array.

Time lags between 8 and 41 days are found in the correlations. This means that the advection velocity for the 550 km distance between the arrays was between 16 cm/s and 80 cm/s. Voet and Quadfasel (2010) found DSOW plume velocity between the Denmark Strait sill and Ammassalik between 20 cm/s and 65 cm/s with a mean velocity of 45 cm/s. Most of the time lags indicate velocities within this range. The resulting time lags therefore lie within the expected range.

Table 7: *Salinity correlation of the 20 day low pass filtered data from the Ammassalik moorings with the data from Denmark Strait moorings DS1 and DS2. Only significant correlation coefficients are shown.*

2008-2009	**F2New**	**UK1**	**G1**	**UK2**
DS1	-	-	-	-
DS2	-	-	-	0.17**@**25days
2009-2010	**F2New**	**UK1**	**G1**	**UK2**
DS1	0.15**@**9days	negative	-	negative
DS2	0.38**@**17days	0.32**@**17days	-	0.44**@**18days
2010-2011	**F2New**	**UK1**	**G1**	**UK2**
DS1	0.34**@**19days	0.26**@**21days	0.25**@**22days	0.28**@**20days
DS2	-	-	-	-
2011-2012	**F2New**	**UK1**	**G1**	**UK2**
DS1	0.25**@**31days	negative	negative	negative
DS2	0.35**@**37days	0.17**@**39days	0.16**@**38days	0.40**@**36days

The correlation coefficient with the corresponding time lag for salinity of every mooring combination is shown in Table 7. One fourth of these salinity correlations are negative. The rest has coefficients between 0.15 and 0.34 for correlations with DS1 and 0.16 to 0.44 for correlations with DS2. As seen in potential temperature better correlations can be found with the DS2 data. Except of the period 2010-2011 no high correlations can be found with the DS1 data. The best correlation can be found with the F2New data

with a coefficient of 0.34 and a time lag of 19 days. The best correlations for DS2 can be found with the UK2 data with a maximum coefficient of 0.44 and a time lag of 18 days. The time lag varies between 9 and 39 days with no tendency. The salinity correlation coefficients are much smaller than the ones within the arrays. The salinity has to be influenced strongly by entrainment.

Advection is therefore not the main reason for extreme events present at the Ammassalik array. Entrainment plays an important role, especially for salinity variability. It is now important to identify the entrained water masses and their content to the changes in variability of the DSOW.

4.3 Summary and discussion

The DSOW potential temperature time series of the Denmark Strait and Ammassalik array show good correlation. Hence, the DSOW temperature variability is not strongly influenced by entrainment. Temperature signals are advected from the Denmark Strait to the Ammassalik array. But the potential temperature of the DSOW increases on the way south around $1 - 2°C$. The increasing temperature can partly be explained by crossing eddies, which occur regularly and are warming the DSOW around $1°C$ (Voet and Quadfasel, 2010).

Most of the potential temperature correlations can be found between 10 and 20 days time lag. This gives advection velocities between 65 cm/s and 31 cm/s. These velocities are in the velocity range for the DSOW plume found by Voet and Quadfasel (2010).

The DSOW salinity variability is different between the Denmark Strait and Ammassalik array. The variability of the DSOW salinity time series is small at the Denmark Strait. At the Ammassalik array the salinity variability of the DSOW is larger than in the Denmark Strait. While the mean salinity of the DSOW is not changing between the Denmark Strait and Ammassalik array, variability is added. Entrainment into the DSOW highly influences the salinity variability. Salinity signal are hence not advected from the Denmark Strait and can therefore not be seen in the DS mooring data. To find out more about freshening events occurring at the Ammassalik array, the entrained water masses as well as their variability have to be analyzed.

5 Entrainment into the DSOW

The DSOW properties are changed by entrainment of ambient water masses during the descending of the plume. All potential temperature and density data shown in this chapter are calculated for a reference pressure of 3000 dbar to make them comparable to other measurements. Ambient water masses which can be entrained into the DSOW are identified. A water mass analysis is done to approximate their volume content to the DSOW measured at the Ammassalik array.

5.1 Property changes in the DSOW

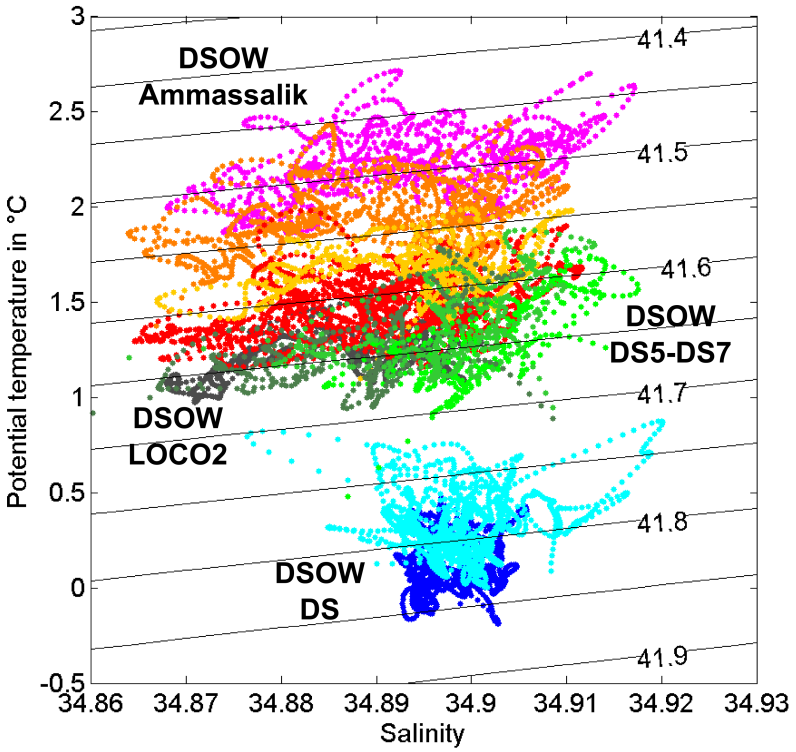

Figure 30: *T-S diagram of the DSOW at the moorings DS1 (blue), DS2 (cyan), DS5-DS7 (green colors), F2New (magenta), UK1 (dark orange), G1 (yellow), UK2 (red) and LOCO2 (dark grey) for the 20 day low pass filtered data. The thin black lines indicate the density levels for a reference pressure of 3000 dbar.*

To study mixing processes temperature and salinity relations are a useful tool. Figure 30 shows the T-S diagram for the DSOW measured at the Denmark Strait, LOCO and Ammassalik moorings for the 20 day low pass filtered data. The density of the DSOW decreases on the way south. The densest water mass is the DSOW at the Denmark Strait sill (blue colored). The potential temperature is $1°C$ to $2°C$ colder than at LOCO2 and the Ammassalik moorings. The DSOW measured at the LOCO2 mooring (dark grey) fits to the DSOW found at the Ammassalik array (red colors). Between these two locations the density is stable and increasing with depth. All Ammassalik data show a similar range of salinity, but their potential temperature is decreasing with depth from the shallow F2New mooring (magenta) to the deep UK2 mooring (red). The DSOW at DS5-DS7 is $0.5°C$ to $1.5°C$ warmer than the DSOW at the sill. The DS5-DS7 data show a salinity range of $34.865 - 34.915$ *psu* similar to the Ammassalik array. The potential temperature is between $1°C$ and $1.8°C$ which is partly in the range of the DSOW measured at UK2 and partly lower.

The DSOW at LOCO2 shows nearly the same range of salinity as the Ammassalik data but the corresponding temperatures are in a smaller range. The same can be seen for the Ammassalik data compared with the DS5-DS7 data. Voet (2006) found strongest entrainment in the first 200 km downstream of the Denmark Strait sill. The data from 2007-2012 indicate strong entrainment during the first 100 km downstream. The entrained water masses warm the DSOW and also add salinity variability to the DSOW during the descending. Water masses present in layers close to the DSOW especially in the first 100 km downstream of the Denmark Strait sill have to be identified to explain the hydrographic changes in the DSOW properties.

5.2 Entrained water masses

The low salinity lid can not be the reason for lower salinities found in the DSOW further south. Strongest entrainment occurs in the first 100 km downstream of the Denmark Strait sill. The low salinity lid can also be found as a cap over the DSOW beyond 2000 m between $64 - 65°N$ (Rudels et al., 1999), which is approximately 300 km south of the sill.

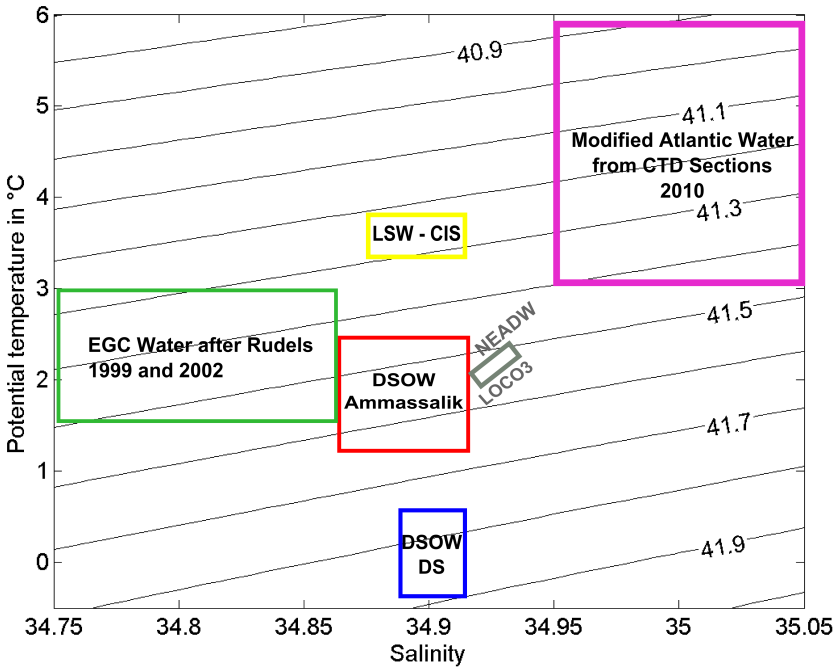

Figure 31: *T-S diagram with all contributing water masses to the entrainment into the DSOW. The water masses are shown as boxes.*

Ambient water masses which can be entrained into the DSOW on the way south are Labrador Sea Water (LSW) and North East Atlantic Deep Water (NEADW) (Dickson et al., 2008). The NEADW measured at the LOCO3 mooring is in a higher temperature range as the DSOW at the Denmark Strait sill with higher salinities (Figure 31). The LSW measured at the CIS mooring is $2-3°C$ warmer than the DSOW but within the same salinity range. They can not explain the mixing in the first 100 km after the sill because the LSW could not be found close to the Denmark Strait sill and the NEADW layer is to deep to mix within 500-1500 m depth.

Water masses which could influence the DSOW close to the sill are the water transported by the East Greenland Current (EGC) and Atlantic waters. Rudels et al. (1999) and Rudels et al. (2002) pointed out that water from the EGC with low salinity but high density may cross the shelf break south of the Denmark Strait sill. South of the Denmark Strait sill a few deep troughs exist, which are cutting into the Greenland slope. Through

these channels dense EGC water with low salinity can sink into the deep Irminger Sea and thereby be entrained into the DSOW. This observed flow is also called the East Greenland Spill Jet (Pickart et al., 2005). Falina et al. (2012) showed that the shelf water cascading into the Irminger Sea is probably an episodic and local phenomenon. They found EGC waters at a depth of $260 - 370$ m approximately 200 km southwest of the Denmark Strait sill and approximately 400 km south of the sill in 1400 m depth with warmer temperatures than close to the sill but still with low salinities.

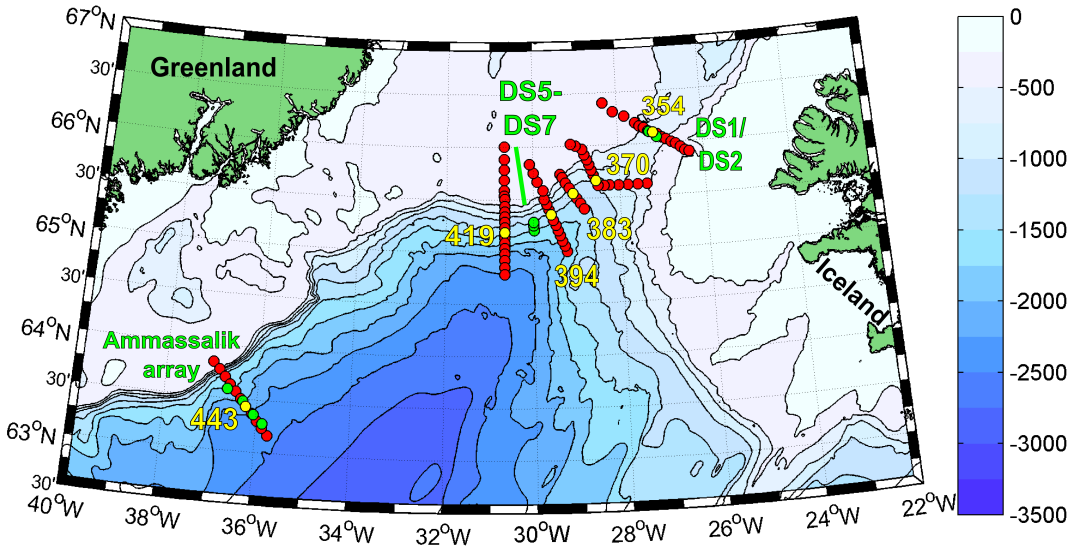

Figure 32: *CTD sections from the cruise M82/1 (red) in July 2010. Mooring locations are shown in green. The chosen stations for a section along the shelf between DS sill and Ammassalik are highlighted in yellow. The station number are given as well.*

The properties of the entrained Atlantic Water are derived from CTD sections between the Denmark Strait sill and Ammassalik array taken in 2010 (M82/1). Figure 32 shows the CTD sections (red) of the M82/1 cruise in July 2010. To determine the water which is available for entrainment into the DSOW, a section along the Greenland shelf (yellow) is chosen.

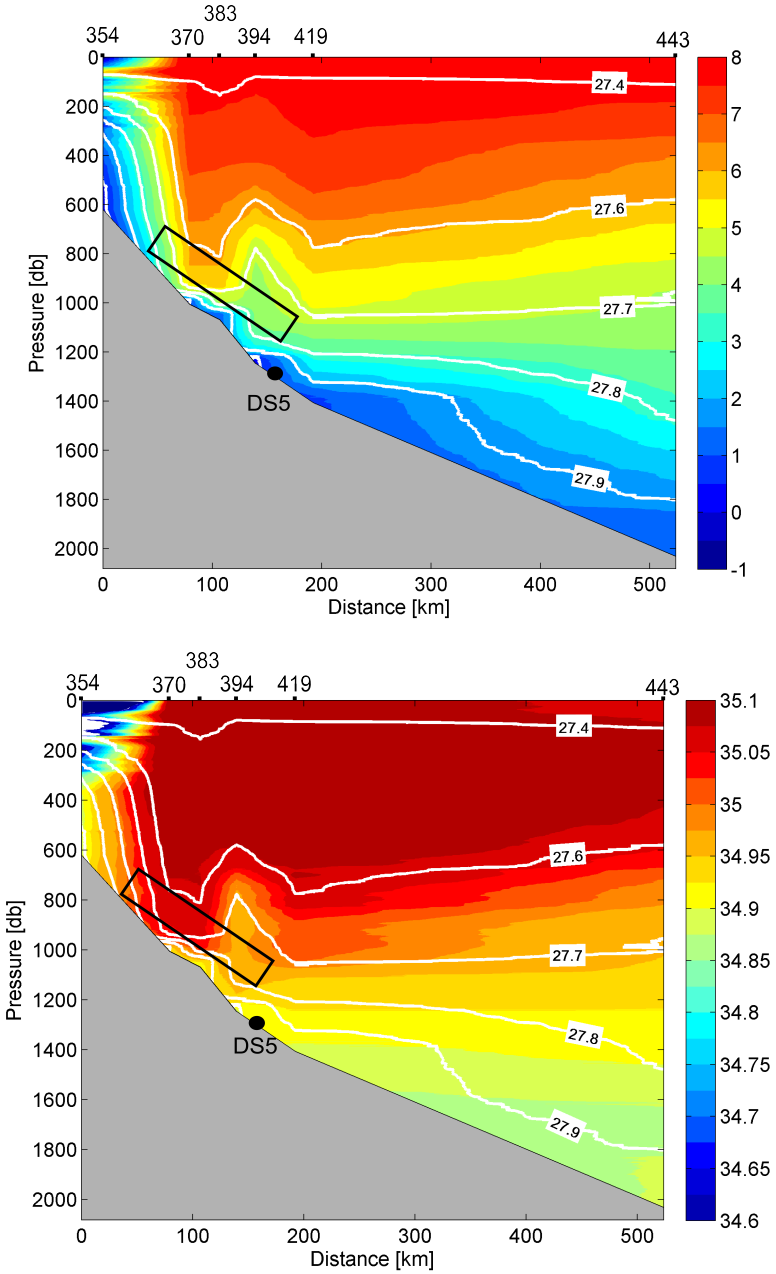

Figure 33: *Potential temperature (top) and salinity (bottom) section along the Greenland shelf from the sill (left) to Ammassalik (right) CTD stations of the M82/1 cruise in July 2010. The locations of the CTD stations can be seen in Figure 32. Black dots at the top of the figure indicate the position where CTD measurements were taken. The black box marks water which can be entrained into the DSOW plume.*

Figure 33 shows the potential temperature (top) and salinity (bottom) at the section along the shelf. Warm and salty modified Atlantic water can be identified close to the Denmark Strait sill near the 27.8 kg/m^3 isopycnal. The black box shows the modified Atlantic water which contributes to the entrainment into the plume. The properties of this water change along the region of high entrainment between $3°C$ to $6°C$ in potential temperature and $34.95 - 35.05$ *psu* in salinity.

5.3 Contents of the entrained water masses

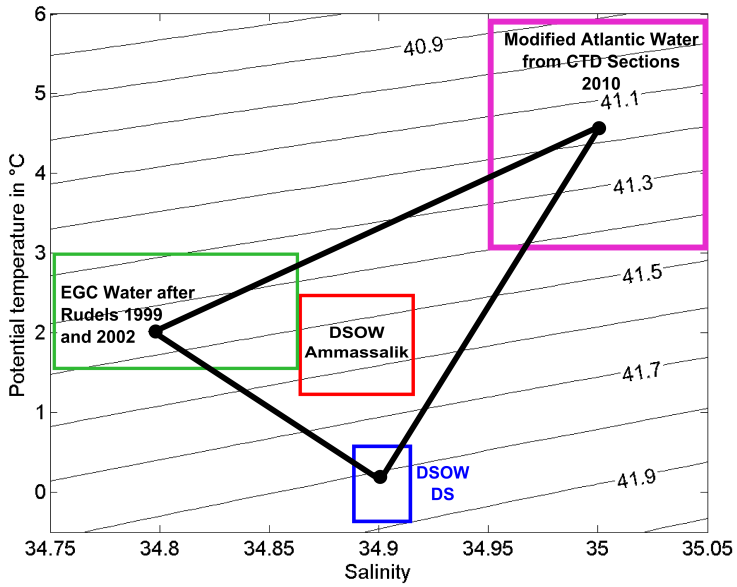

Figure 34: *T-S diagram with all contributing water masses to the entrainment into the DSOW used for content calculations. The water masses are shown as boxes. The chosen mixing triangle is shown in black.*

One of the oldest and best known methods for determining the amounts of different water masses to measured hydrographic properties is the mixing triangle, which is explained in more detail in Chapter 2.4.5. The DSOW - as measured at Ammassalik - can be entirely explained by the mixing from DSOW at the Denmark Strait sill with EGC water and modified Atlantic water. The DSOW at the Denmark Strait sill is defined as $0.3°C$ and 34.9 *psu*. This is the mean salinity and temperature value of the DS2 data. The DS2

data are chosen because the correlations in temperature and salinity showed better results than the ones with DS1 (Chapter 4.2). The EGC water is defined as $2°C$ and 34.8 *psu* after Falina et al. (2012). The Atlantic water is defined as $4.5°C$ and 35 *psu* which are the mean properties of the Atlantic water at overflow depth close to the Denmark Strait sill as described in Chapter 5.2. The resulting water mass is the DSOW measured at the Ammassalik moorings. Figure 34 shows all used water masses as boxes and the mixing triangle used in this chapter.

Table 8 shows the mean volume contents and standard deviations for the mixed water masses creating the DSOW measured at the Ammassalik moorings. The time periods for calculation differ due to available salinity time series. Figure 35 shows the contents of mixed water masses for the time period 2009-2012.

Table 8: *Mean source water content and standard deviation of the mixed water masses to create DSOW measured at the Ammassalik moorings. The contents are calculated for the time periods 2009-2012 for F2New and UK1, 2010-2012 for G1 and 2007-2012 for UK2 measurements.*

	Mean content ± std [%]		
	DSOW at DS sill	**Atlantic water**	**EGC water**
F2New	32 ± 6	31 ± 5	37 ± 7
UK1	39 ± 6	25 ± 5	36 ± 7
G1	51 ± 5	22 ± 4	27 ± 6
UK2	56 ± 5	17 ± 4	27 ± 7

The volume content of the DSOW from the Denmark Strait sill increases at the Ammassalik moorings with increasing depth. The standard deviation has a similar magnitude for all depth. The DSOW from the sill provides the largest volume content of the DSOW measured at the Ammassalik moorings except of the DSOW measured at the shallow F2New mooring. Here the EGC water provides the largest volume content. At the shallow mooring the DSOW from the sill and Atlantic water provide similar volume contents. The EGC water provides the largest volume content of entrained waters at all moorings. This can be a result of a longer path along shallower parts of the shelf, so that more EGC can be mixed into the plume. The EGC water content decreases with depth but not as consistent as it can be seen in the Atlantic water content. At the shallower F2New and

UK1 moorings a higher volume content of EGC water can be seen than at the deeper G1 and UK2 moorings. This is opposite of what can be seen for the original DSOW. The volume contents within these two steps are in the same order as well as the standard deviation. The standard deviations at the shallower moorings are 0.5-1% higher than at the deeper moorings. The volume content of modified Atlantic water contributing to the DSOW is decreasing with depth. The standard deviations are in the same range as seen for the DSOW at the sill. In all depth the modified Atlantic water provides the smallest volume content of all mixed water masses.

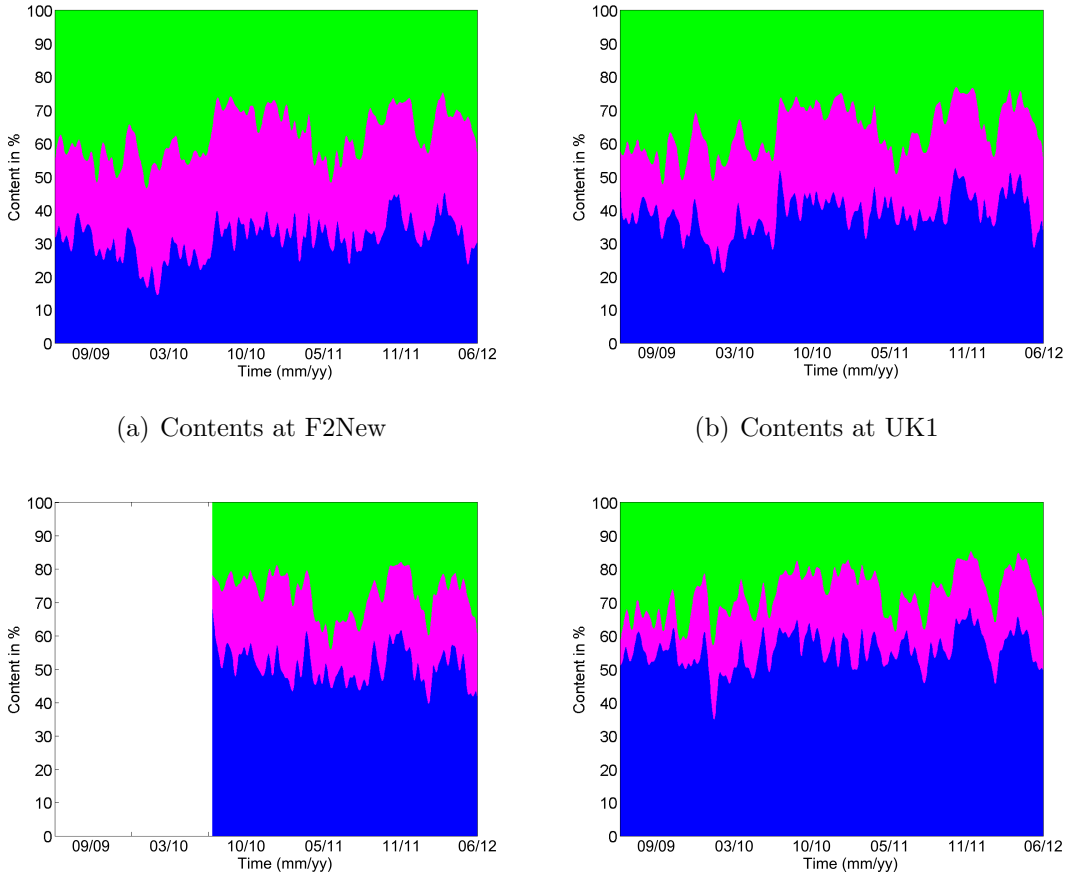

(a) Contents at F2New

(b) Contents at UK1

(c) Contents at G1

(d) Contents at UK2

Figure 35: *Volume contents in % of original DSOW from the DS sill (blue), modified Atlantic water (magenta) and EGC water (green) giving the DSOW measured at the Ammassalik moorings F2New (a), UK1 (b), G1 (c) and UK2 (d) for the time period 2009-2012.*

The maximum standard deviation occur for the EGC water. Maxima of EGC water content can be found in nearly monthly intervals (Figure 35). They can be found at all moorings in the array at the same time. This fits to the assumption of Falina et al. (2012), that the EGC water is just episodically and locally cascading into the deeper layers and then mixing into the DSOW. Maxima of Atlantic water content can be found every second month. Sometimes the intervals are longer. An exactly regular interval can not be found for all water masses. The DSOW is highly influenced by EGC water due to the higher volume contributing to the mixing than the Atlantic water. This would also explain the low salinities found at the Ammassalik moorings.

5.4 Summary and discussion

The Labrador Sea water has the same range of salinities as the DSOW at the Ammassalik array, but higher potential temperatures. Thus, it can influence the temperature of the DSOW from the sill by entrainment but not the variability in salinity. The NEADW is in the same temperature range as the DSOW at Ammassalik with slightly higher salinities. Temperature changes can therefore not be explained by entrainment of NEADW. Due to the higher salinities than the original water, low salinities at Ammassalik can also not be explained. Half of the salinity range found at the Ammassalik array can not be explained by mixing with LSW and NEADW.

The entrainment can be separated into two regions. The first 100 - 200 km south of the Denmark Strait sill, as before described by Voet (2006), and entrainment in deeper layers further south. In the first part Atlantic water and water transported by the EGC can be found. Further south LSW and NEADW is entrained. Entrainment of the warm and salty Atlantic water and the fresh EGC water can explain the whole range of temperature and salinity changes in the DSOW.

More DSOW from the sill is present at the deep moorings in the Ammassalik array. The entrained Atlantic water provides the lowest volume content of DSOW at Ammassalik. Due to its high salinities entrainment can not explain the salinity minima found at the Ammassalik array. The higher temperatures of the Atlantic Water can explain the warming of the plume during the first 100 km south of the sill. The EGC provides the largest

volume content of entrained water. The EGC is in the same temperature range as the DSOW at the Ammassalik array with lower salinities. Changes in the EGC can therefore strongly influence the salinity variability. Salinity minima can result from higher entrainment rates of EGC water.

These results are an estimate of the entrainment into the DSOW plume. Changes of $\pm 0.5°C$ oder ± 0.05 *psu* in the definition of the points used for calculations with the mixing triangle can cause deviations of up to 20% in volume content of each water mass. Also, probably more than three water masses are mixing which makes an analysis with additional tracer data (like oxygen, nitrate, phosphate or others) necessary. An optimum multiparameter analysis therefore has to be done to solve this question. Also temperature and salinity time series of EGC water and Atlantic water close to the entrainment region would be helpful to evaluate the source of the low salinity signals.

6 Conclusion

Previous studies suggested that the hydrographic signals in the DSOW at Ammassalik were a result of changes in source water properties which are feeding the DSOW north of the Denmark Strait sill. Most of these results were based on modeling studies because no moorings at the Denmark Strait sill were measuring temperature and salinity. In 2005 moorings at the Denmark Strait sill were equipped with MicroCATs to fill this gap. Temperature and salinity data between 2007 to 2012 from the Denmark Strait sill and Ammassalik array are analyzed in this thesis to answer some of the still remaining questions about the DSOW.

Can the freshening trend detected by Dickson et al. (2002) also be seen in the data between 2007 and 2012?
The trend to lower salinities of the DSOW found by Dickson et al. (2002) did not continue in the 2007-2012 period. The annual mean salinity values between 2007 and 2012 are higher than the annual mean salinity values between 1993 and 2001. The mean values differ at each mooring location and each year of measurement, which represents interannual variability. A salinity minimum found in July 2009 can therefore be part of a multi-year cycle. Short time series of a few years can cause misinterpretation of interannual variability as long term trends. Thus longer time series are necessary to identify interannual and decadal variability.

What kind of variability occured in salinity and temperature between 2007 and 2012 at the Ammassalik array?
High variability on short time scales is present at all moorings. Part of this variability is a result of crossing eddies. In all power spectra no dominant frequency is evident. A significant seasonal cycle can be detected in all time series, but can only explain up to 10% of the variance. This result corresponds with the magnitudes of the annual cycles detected by Jochumsen et al. (2012) at the Denmark Strait sill and by van Aken and de Jong (2012) near Cape Farewell. The magnitude of the annual cycle is preserved from the Denmark Strait sill to Cape Farewell. This supports the assumption from van Aken and de Jong (2012) that it originates from forcing by the atmosphere of DSOW source waters. To detect influences of climate change, longer time series are nescessary to identify longer periods and dominant frequencies.

Did extreme events in temperature occur between 2007 and 2012 at Ammassalik and are they advected from the Denmark Strait?
For potential temperature no extreme events can be recognized. The temperature time series of the Denmark Strait and Ammassalik array show good correlation. Temperature signals are advected from the Denmark Strait to the Ammassalik array. Most of the potential temperature correlations can be found between 10 and 20 days time lag. This gives advection velocities between 65 cm/s and 31 cm/s. These velocities are in the velocity range for the DSOW plume found by Voet and Quadfasel (2010). But the potential temperature of the DSOW increases on the way south around $1 - 2°C$. The increasing temperature can partly be explained by crossing eddies, which occur regularly and are warming the DSOW around $1°C$ (Voet and Quadfasel, 2010). Hence the DSOW has to be additionally warmed by entrainment while the variability is not changed.

Did extreme events in salinity occur between 2007 and 2012 at the Ammassalik array and are they advected from the Denmark Strait?
Two freshening events can be identified occurring in April to June 2011 and in January 2012. Both events have approximately half the amplitude of the ones found in 1999 and 2004 by Dickson et al. (2008). The freshening events present in the Ammassalik time series are not seen in the Denmark Strait measurements. At the Ammassalik array the salinity variability of the DSOW is larger than at the Denmark Strait. While the mean salinity of the DSOW is not changing between the Denmark Strait and Ammassalik array, variability is added. Salinity signals are hence not advected from the Denmark Strait and can therefore not be seen in the DS mooring data. Entrainment into the DSOW highly influences the salinity variability. This rejects the hypotheses of Holfort and Albrecht (2007) and Hall et al. (2011) that the DSOW salinity variability is resulting from changes of the source water masses north of the Denmark Strait sill and is advected to the south within the DSOW plume.

Which water masses have to be entrained into the DSOW to change the salinity and temperature variability of the plume?
The Labrador Sea Water has the same range of salinities as the DSOW at the Ammassalik array but higher potential temperatures. Thus it can influence the temperature of the DSOW from the sill by entrainment but not the variability in salinity. The NEADW is in

the same temperature range as the DSOW at Ammassalik with slightly higher salinities. Half of the salinity range found at the Ammassalik array can not be explained by mixing with LSW and NEADW. In contrast, entrainment of the warm and salty Atlantic water and the fresh EGC water closer to the Denmark Strait sill can explain the whole range of temperature and salinity changes in the DSOW. Jochumsen et al. (2012) revealed that the Atlantic inflow can reach the bottom of the Denmark Strait and nearly fill the passage in the sill. Atlantic water can therefore highly influence the entrainment into the DSOW plume.

A estimate of the contents of the entrained water masses can be obtained by the mixing of DSOW from the sill with EGC water and modified Atlantic water. More DSOW from the sill is present at the deep moorings in the Ammassalik array. The entrained Atlantic water provides the lowest volume content of DSOW at Ammassalik. The higher temperatures of the Atlantic Water can explain the warming of the plume. The EGC provides the largest volume content of entrained water. The EGC is in the same temperature range as the DSOW at the Ammassalik array with lower salinities. Salinity minima can result from higher entrainment rates of EGC water. Hall et al. (2011) pointed out that the EGC is important for modifying the salinity of the DSOW. The new results support this statement. But contrary to Hall et al. (2011) the results presented here show that this modifying is happening via entrainment south of the Denmark Strait sill. Temperature and salinity time series of EGC water and Atlantic water close to the entrainment region would be helpful to evaluate the source of the low salinity signals more accurately.

On the way to Ammassalik, probably more than three water masses are mixing into the DSOW plume. A three point mixing triangle can thus not be used to recalculate the contents of all contributing source water masses from salinity and potential temperature data alone. Therefore an optimum multiparameter analysis has to be done. Additional tracer like oxygen, nitrate or phosphate are needed for this analysis. Measuring additional tracers at the mooring arrays would help to identify all entrained water masses.

7 Appendix

7.1 Seasonal cycle

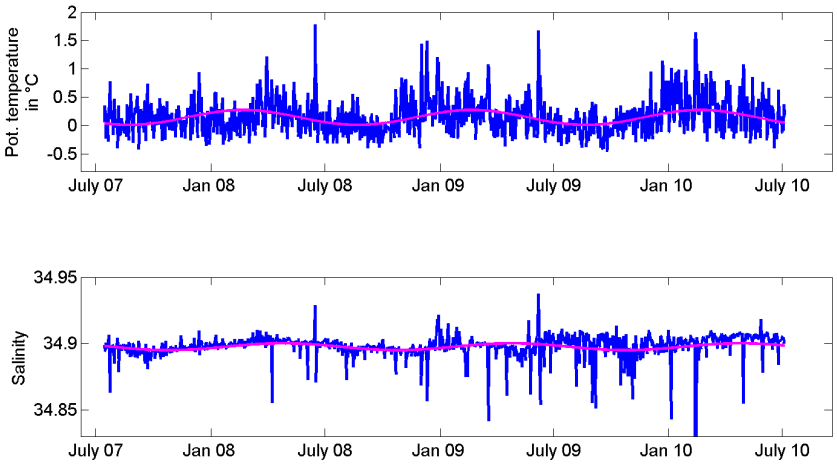

Figure 36: *Seasonal cycle (magenta) at DS2 for potential temperature (top) and salinity (bottom). The daily mean time series is shown in blue.*

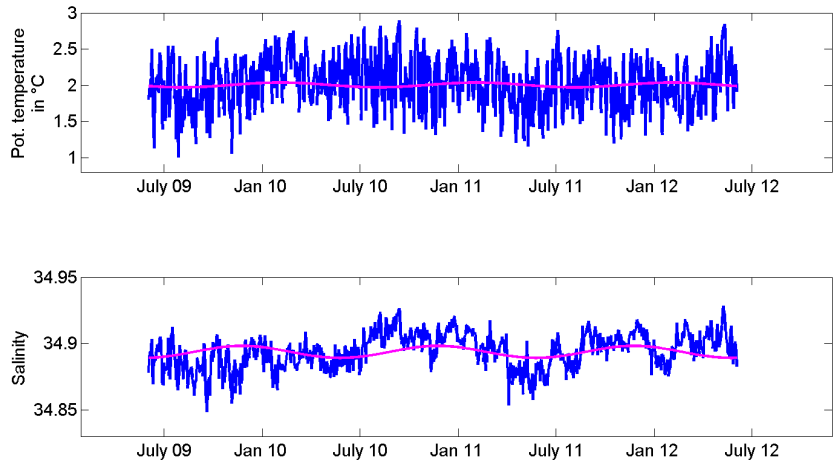

Figure 37: *Seasonal cycle (magenta) at F2 for potential temperature (top) and salinity (bottom). The daily mean time series is shown in blue.*

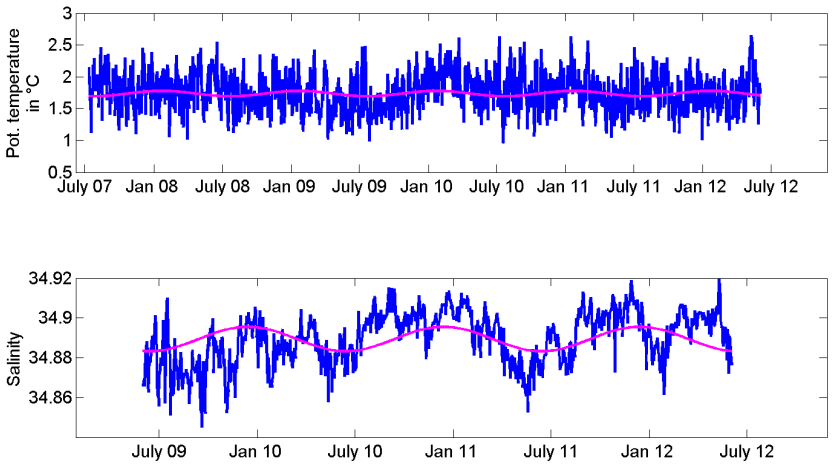

Figure 38: *Seasonal cycle (magenta) at UK1 for potential temperature (top) and salinity (bottom). The daily mean time series is shown in blue.*

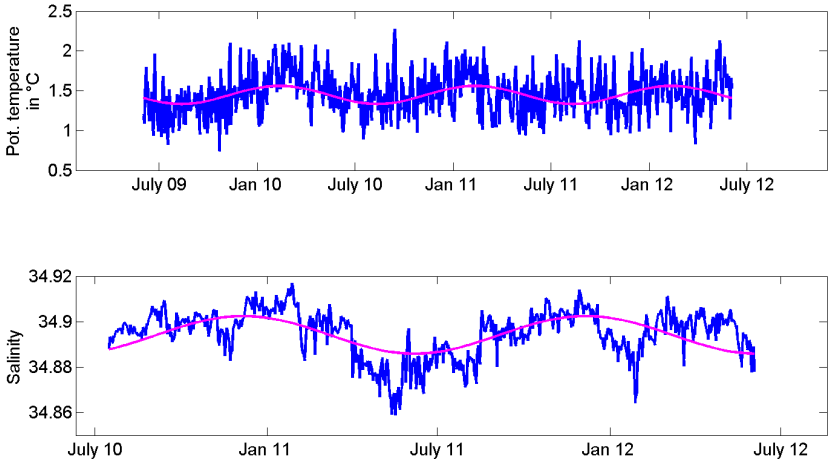

Figure 39: *Seasonal cycle (magenta) at G1 for potential temperature (top) and salinity (bottom). The daily mean time series is shown in blue.*

7.2 Ammassalik correlations

To get a better overview for the potential temperature and salinity correlations, all correlation were done for every measuring period. The results are shown in Table 7.2. The possible correlation time periods can be seen in Figure 28 and 29 in chapter 4.1.

Table 9: *Correlation of the Ammassalik moorings for different measuring periods*

(a) Correlation of pot. temperature

2007-2008	**UK1**	**G1**	**UK2**
UK1	-	-	0.45
2008-2009	**UK1**	**G1**	**UK2**
UK1	-	-	0.77
2009-2010	**UK1**	**G1**	**UK2**
F2New	0.91	0.63	0.53
UK1	-	0.77	0.65
G1	-	-	0.91
2010-2011	**UK1**	**G1**	**UK2**
F2New	0.91	0.58	0.50
UK1	-	0.73	0.60
G1	-	-	0.87
2011-2012	**UK1**	**G1**	**UK2**
F2New	0.89	0.54	0.47
UK1	-	0.64	0.42
G1	-	-	0.77

(b) Correlation of salinity

2007-2008	**UK1**	**G1**	**UK2**
UK1	-	-	-
2008-2009	**UK1**	**G1**	**UK2**
UK1	-	-	-
2009-2010	**UK1**	**G1**	**UK2**
F2New	0.91	-	0.79
UK1	-	-	0.88
G1	-	-	-
2010-2011	**UK1**	**G1**	**UK2**
F2New	0.98	0.92	0.87
UK1	-	0.97	0.93
G1	-	-	0.97
2011-2012	**UK1**	**G1**	**UK2**
F2New	0.92	0.82	0.71
UK1	-	0.92	0.78
G1	-	-	0.90

References

Aandera (2002). Aandera Doppler Current Meter RCM 11 Data Sheet D 331. STATE-OF-THE-ART SCIENTIFIC PRODUCTS, http://www.comm-tec.com/Prods/mfgs/Aanderaa/Brochures/RCM%2011%20D331.pdf.

De Jong, F. (2010). *Hydrographic Variability of the Irminger Sea*. Ph. D. thesis, University of Utrecht, Netherlands.

Dickson, B., S. Dye, S. Jónsson, A. Köhl, A. Macrander, M. Marnela, J. Meincke, S. Olsen, B. Rudels, H. Valdimarsson, and G. Voet (2008). *Arctic-Subarctic Ocean Fluxes*, Chapter 19: The Overflow Flux West of Iceland: Variability, Origins and Forcing, pp. 443–474. Springer.

Dickson, R. and J. Brown (1994). The production of North Atlantic Deep Water: Sources, rates and pathways. *J. Geophys. Res. 99*(C6), 12,319–12,341.

Dickson, R., I. Yashayaev, J. Meincke, W. Turrell, S. Dye, and J. Holfort (2002). Rapid Freshening of the Deep North Atlantic over the past Four Decades. *Nature Lond. 416*, 832–837.

Emery, W. and R. Thomson (2004). *Data Analysis Methods in Physical Oceanography*. ELSEVIER.

Falina, A., A. Sarafanov, H. Mercier, P. Lherminier, A. Sokov, and N. Daniault (2012). On the cascading of dense shelf waters in the Irminger Sea. Journal of Physical Oceanography, doi:10.1175/JPO-D-12-012.1. in press.

Fogelqvist, E., J. Blindheim, T. Tanhua, S. Østerhus, E. Buch, and F. Rey (2003). Greenland-Scotland overflow studied by hydro-chemical multivariate analysis. *Deep Sea Research 50*, 73–102.

Friedrichs, A. (2011). The Overflow in the Faroe Bank Channel - A frequency analysis. Master's thesis, University of Hamburg.

Hall, S., S. Dye, K. Heywood, and M. Wadley (2011). Wind forcing of salinity anomalies in the Denmark Strait overflow. *Ocean Science 7*, 821–834.

Hansen, B., S. Østerhus, D. Quadfasel, and W. Turrell (2004). Already the Day After Tomorrow? *Science 305*, 953–954, doi:10.1126/science.1100085.

Holfort, J. and T. Albrecht (2007). Atmospheric forcing of DSOW salinity. *Ocean Science 3*, 411–416.

Jochumsen, K., D. Quadfasel, H. Valdimarsson, and S. Jonsson (2012). Variability of the Denmark Strait overflow: moored time series from 1996-2011. Journal of Geophysical Research, accepted.

Kanzow, T., S. Cunningham, D. Rayner, J. Hirschi, W. Johns, M. Baringer, H. Bryden, L. Beal, C. Meinen, and J. Marotzke (2007). Observed Flow Compensation Associated with the MOC at 26.5°N in the Atlantic. *SCIENCE 317*, 938–941.

Käse, R. H., J. Girton, and T. B. Sanford (2003). Structure and variability of the Denmark Strait Overflow: Model and Observations. *Journal of Geophysical Research 108*, No. C6.

Macrander, A., R. H. Käse, U. Sønd, H. Valdimarsson, and S. Jónsson (2007). Spatial and temporal structure of the Denmark Strait Overflow revealed by acoustic observations. *Ocean Dynamics 57*, 75-89.

McCartney, M. S., R. Curry, and H. Bezdek (1997). The interdecadal warming and cooling of Labrador Sea Water. *ACCP Notes IV,1*, 1–11.

Moritz, M. (2011). Der Einfluss mesoskaliger Wirbel auf Strömungsmessungen des Overflows in der Dänemarkstrasse. Bachelor's thesis, University of Hamburg.

Pickart, R., D. Torres, and P. Fratantoni (2005). The East Greenland spill jet. *Journal of Physical Oceanography 35*, 1037–1053.

Ross, C. (1984). Temperature-salinity characteristics of the 'overflow' water in Denmark Strait during 'OVERFLOW'73'. *Rapp. P.V. Fisheries. Reun. Cons. Int. Explor. Mer. 185*, 111–119.

Rudels, B., P. Eriksson, H. Grönvall, R. Hietala, and J. Launiainen (1999). Hydrographic Observations in Denmark Strait in Fall 1997, and their Implications for the Entrainment into the Overflow Plume. *Geophysical Research Letters 26, No.9*, 1325–1328.

Rudels, B., E. Fahrbach, J. Meincke, G. Budeus, and P. Eriksson (2002). The East Greenland Current and its contribution to the Denmark Strait overflow. *Journal of Marine Science 59*, 1113–1154.

Schönwiese, C. (2006). *Praktische Statistik für Meteorologen und Geowissenschaftler*. Gebrüder Borntraeger.

Talley, L., G. Pickard, W. Emery, and J. Swift (2011). *Descriptive Physaical Oceanography: An introduction*. Elsevier.

Tanhua, T., K. Olsson, and E. Jeansson (2005). Formation of Denmark Strait overflow water and its hydro-chemical composition. *Journal of Marine Systems 57*, 264–288.

Tanhua, T., K. Olsson, and E. Jeansson (2008). *Arctic-Subarctic Ocean Fluxes*, Chapter 20: Tracer Evidence of the Origin and Variability of Denmark Strait Overflow Water, pp. 475–503. Springer.

Tomczak, M. (1981). A multi-parameter extension of temperature/salinity diagram techniques for the analysis of non-isopycnal mixing. *Progress in Oceanography 70*, 147-171.

Torrence, C. and G. Compo (1998). A Practical Guide to Wavelet Analysis. *Bulletin of the American Meteorological Society 791*, 61-78.

van Aken, H. and F. de Jong (2012). Hydrographic variability of Denmark Strait Overflow Water near Cape Farewell with multi-decadal to weekly time scales. *Deep Sea Research I 66*, 41–50.

Voet, G. (2006). Entrainment in the Denmark Strait Overflow Plume by meso-scale Eddies. Diplomarbeit, University of Hamburg.

Voet, G. and D. Quadfasel (2010). Entrainment in the Denmark Strait overflow plume by meso-scale eddies. *Ocean Science 6*, 301–310.

Whitehead, J. (1998). Topographic control of oceanic flows in deep passages and straits. *Reviews of Geophysics 36*, 423-440.

Acknowledgements

I'd like to thank

- Professor Dr. Detlef Quadfasel for all comments and ideas to this thesis which were a great help. Additionally for the opportunity to work as a research student in his group for more than 3 years with several research cruises.
- Dr. Kerstin Jochumsen for outstanding support (especially for calibrating the mooring data), constant guidance, inspiring discussions and for all the time spending with answering my questions.
- Dr. Stephen Dye and Neil Needham for providing me with the most recent and unpublished mooring data and a lot of interesting and enthusiastic discussions.
- Dr. Hendrik M. van Aken for the LOCO data and an interesting discussion about entrainment and mooring measurements.
- Dr. Johannes Karstensen for the CIS data and an excellent cruise in my research area.
- Nuno Nunes for the DS5-DS7 data and a lot of interest in my work.
- Anna Friedrichs for helping me with all the wavelet stuff and correlations, and for enthusiastic discussions during lunch times.
- Theresa Reichelt for making me smile everytime I was stressed and creating a comfortable working atmosphere in our office.

I'd also like to thank my parents Lilli und Michael Köllner and my aunt Maja Köllner for supporting and encouraging me. Many thanks to my boyfriend Hauke Lehmann for being with me and backing me up in all times!

This thesis is based on THOR data. THOR ("Thermohaline Overturning- At Risk?") is a project financed by the European Commission through the 7th Framework Programme for Research, Theme 6 Environment, Grant agreement 212643.

Eigenständigkeitserklärung

Hiermit versichere ich, dass ich die vorliegende Masterarbeit selbständig verfasst und keine anderen als die angegebenen Quellen (insbesondere keine im Quellenverzeichnis nicht benannten Internet-Quellen) und Hilfsmittel verwendet habe und die Arbeit von mir vorher nicht in einem anderen Prüfungsverfahren eingereicht wurde. Die eingereichte schriftliche Fassung entspricht der auf dem elektronischen Speichermedium.

Ich bin damit einverstanden, dass meine Masterarbeit veröffentlicht wird.

Hamburg, den 30. Oktober 2012

Manuela Köllner